

Multiscale change point detection via gradual bandwidth adjustment in moving sum processes

Tijana Levajković and Michael Messer*

Vienna University of Technology

Abstract

A method for the detection of changes in the expectation in univariate sequences is provided. Moving sum processes (MOSUM) are studied. These rely on the selection of a tuning bandwidth. Here, a framework to overcome bandwidth selection is presented – the bandwidth adjusts gradually. For that, MOSUM are made dependent on both time and the bandwidth: the domain becomes a triangle. On the triangle, paths are constructed which systematically lead to change points. An algorithm is provided that estimates change points by subsequent consideration of paths. Strong consistency for the number and location of change points is shown. Simulation studies corroborate estimation precision and reveal competitiveness with state of the art change point detection methods. A companion R-package `mscp` is made available on CRAN.

Keywords: *change point detection, moving sum, multiscale, gradual bandwidth, mscp.*

MSC subject classifications: 62G20, 62M99.

1 Introduction

We contribute to the field of change point detection in stochastic sequences. Change point detection applies in various research areas, e.g., climatology (Reeves et al., 2007), speech recognition (Rybach et al., 2009), oceanography (Killick et al., 2010), neuroimaging (Aston and Kirch, 2012), virology (Kass-Hout et al., 2012) etc.

We consider T univariate and independent random variables (RVs) X_1, \dots, X_T , that are piecewise identically distributed, with existing $(2+p)$ -th moments ($p > 0$), without parametric assumptions. Multiple change points in expectation form a set C . See Figure 1 (bottom) for an example with $T = 200$, $X_i \sim N(\mu, \sigma^2)$, three change points $C = \{65, 105, 145\}$, and thus four sections with parameters $\mu = 1, 4, 1, -2$ and $\sigma = 1, 0.8, 1, 0.5$, i.e., changes in σ may additionally occur when μ changes.

There is extensive literature that covers changes in expectation, e.g., methods based on likelihood ratios (Fang et al., 2020; Gombay and Horváth, 1994), empirical processes (Holmes et al., 2013; Horváth and Shao, 2007), U -statistics (Döring, 2010; Gombay and Horváth, 2002; Horváth and Hušková, 2005), least-squares (Harchaoui and Lévy-Leduc, 2010; Lavielle and Moulines, 2000) and many more. We mention methodology based on CUSUM-statistics, e.g.,

*corresponding author

by (Berkes et al., 2006; Dehling et al., 2017; Hinkley, 1971; Page, 1954). For a general overview of change point methods see the textbooks of Chen and Gupta (2000); Brodsky (2017); Csörgő and Horváth (1997). In this paper, we aim to tackle multiple change points that may occur on different time scales, as considered e.g., in Fryzlewicz (2014); Matteson and James (2014); Pein et al. (2017); Spokoiny (2009). We study MOSUM, see e.g., Antoch and Hušková (1999); Chu et al. (1995); Hušková and Slabý (2001); Steinebach and Eastwood (1995). For that we select a window size (bandwidth) $h \in \{1, \dots, \lfloor T/2 \rfloor\}$ and define MOSUM $(D_{t,h})_t$ for index $t = h, \dots, T-h$: for every time t consider two adjacent windows of size h , left $\{t-h+1, \dots, t\}$ (index ℓ) and right $\{t+1, \dots, t+h\}$ (index r), and set

$$D_{t,h} := \sqrt{h} \cdot \frac{\hat{\mu}_r - \hat{\mu}_\ell}{(\hat{\sigma}_r^2 + \hat{\sigma}_\ell^2)^{1/2}} \quad (1)$$

where $\hat{\mu}_j$ and $\hat{\sigma}_j^2$ denote the mean and empirical variance of the RVs whose indices lie in the windows, $j \in \{\ell, r\}$. $D_{t,h}$ is Welch's t -statistic for two samples of size h . We typically find $|D_{t,h}| \approx 0$ if no change is involved, but $|D_{t,h}| > 0$ if there is a change nearby, $t \approx c \in C$. Thus, change point estimates may be obtained by argmax-estimation, see e.g., Eichinger and Kirch (2018).

A major challenge lies in the choice of the window size h . An h small enough is sensitive to rapid changes when it does not overlap subsequent change points, while a larger h improves detection power of small effects as more RVs are evaluated. But note that h too large may result in overlap of subsequent changes and thus in an estimation bias, or even a failure of detection at all. In order to account for change points that occur on multiple time scales, including rapid changes as well as small effects, methods that combine multiple windows were proposed, see e.g., Cho and Kirch (2022); Messer (2022). They work in two steps: first change point candidates are generated for every single h , and afterwards all sets are merged giving final estimates. Despite improvements, the methods demand the selection of a window set that best accounts for the location of unknown change points.

The aim of this paper is to provide a MOSUM framework that overcomes window selection, but nevertheless exploits multiple windows to address change point occurrences on multiple time scales, denoted *multi-scale change point detection* algorithm (MSCP), see Algorithm 4.5. For that we extend the MOSUM perspective: instead of considering $(D_{t,h})_t$ as a process of time t only, we let it depend on both t and h , i.e., $(D_{t,h})_{(t,h)}$, while the indices (t, h) lie in a triangle $\Delta_\delta \subset \mathbb{R}^2$, see Figure 1 (top). We define $\Delta_\delta := \{(t, h) \mid t \in T_h, h \in H_\delta\}$, for which we consider first $\delta \in \{1, 2, \dots, \lfloor T/2 \rfloor\}$ a fixed minimal window, while $\lfloor \cdot \rfloor$ denotes the floor function, second $H_\delta := [\delta, T/2]$ a window interval, and third $T_h := [h, T-h]$ a time interval. Note, Δ_δ is a right-angled and isosceles triangle, and the hypotenuse is oriented as the lower edge and refers to the smallest window $h = \delta$. A higher horizontal slice refers to a larger h , and the upper vertex describes the largest $h = \lfloor T/2 \rfloor$.

The triangular structure follows from shrinkage of possible t -indices $h, \dots, T-h$ when h increases. In Figure 1 $D_{t,h}$ is color-coded with $D_{t,h} \approx 0$ green, > 0 red, and < 0 blue. At $c_1 = 65$ there is an increase in μ and thus $D_{t,h} > 0$, while at $c_2 = 105$ and $c_3 = 145$ a decrease in μ yields $D_{t,h} < 0$, at least when h is not too large ($h < 40$) such that only a single c_u is overlapped. The upper part of Δ_δ refers to larger h that result in an overlap of multiple change points. The area between c_1 and c_2 is green also for h large, at $(t, h) \approx (85, 70)$, because the

parameters in the first and third section coincide and thus the effects cancel out. In contrast, the area between c_2 and c_3 is dark blue for h large, at $(t, h) \approx (120, 70)$, as both changes at c_2 and c_3 are negative, which amplifies the effect and as a consequence simple argmax estimation would be flawed. Importantly, note that for smaller h large values of $|D_{t,h}|$ concentrate around $c_u \in C$.

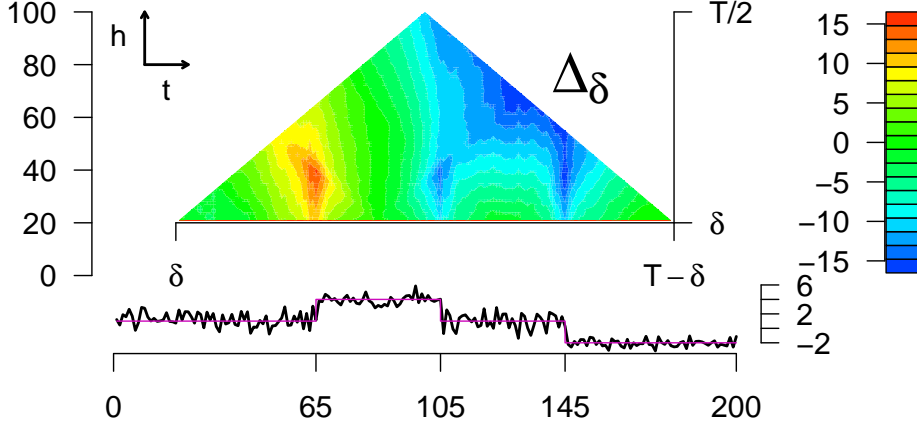


Figure 1: Bottom: Process via $N(\mu, \sigma^2)$ RVs, with $T = 200$, $C = \{65, 105, 145\}$, $\mu = 1, 4, 1, -2$ (pink), $\sigma = 1, 0.8, 1, 0.5$. Top: $D_{t,h}$ with $(t, h) \in \Delta_\delta$ for $\delta = 20$.

MSCP subsequently acts on subsets of Δ_δ by locally exploiting $(D_{t,h})_{(t,h)}$. The key ingredient is the construction of a *zigzag-path*, see Figure 2 (magenta): given a starting value (t_s, h_s) (pink circle), the path leads towards the lower edge of Δ_δ to some point (\hat{c}, δ) , and \hat{c} functions as a change point estimate. The path evolves according to stepwise local argmax-estimation: in each instance the path moves one step downwards, i.e., h switches to $h - 1$ non-randomly. Then the path moves either one step left or right, or it stays, i.e., t switches to some value in $\{t - 1, t, t + 1\}$, while the choice falls on the t -maximizer of $|D_{t,h-1}|$.

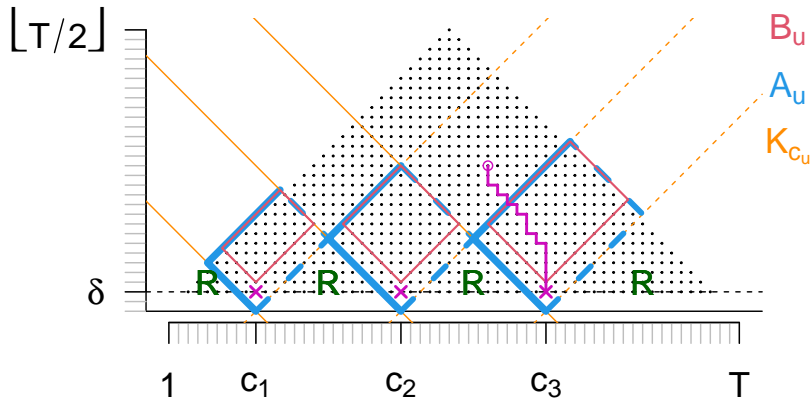


Figure 2: Representation of areas of attraction A_u (blue), inner sets B_u (red), cones K_{c_u} (orange) for three change points c_u , the remainder R (green), and a zigzag-path (magenta).

The idea of MSCP is the following, see also Figure 3: given a set $S \subset \Delta_\delta$ of possible starting values (pink circles), the one maximizing $h^{-1/2} \cdot |D_{t,h}|$ (i.e., the strongest signal to noise ratio) is the first starting point considered. Then its path delivers the first change point estimate \hat{c} . In order to avoid false positives, a breaking criterion is evaluated, which is computed from $D_{t,h}$ on the path. If breaking is not demanded, then \hat{c} is accepted. In order to avoid multiple

detections of the same change point, all elements of S , whose paths could lead to \hat{c} , are deleted from S ('cut out cone'). Then estimation restarts, and iteratively change points are detected until the breaking criterion applies. In Figure 3 the algorithm estimates c_3 , c_1 and c_2 , and then the breaking criterion applies for the next candidate.

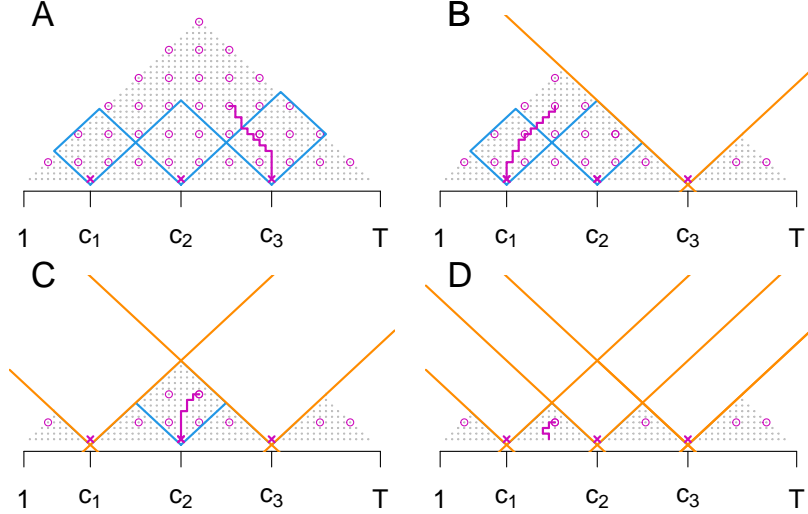


Figure 3: Schematic representation of MSCP. It is $C = \{c_1, c_2, c_3\}$. Subsequently c_3 , c_1 and c_2 are estimated, and then MSCP breaks.

The main result states strong consistency of MSCP for both the number and location of estimated change points. The crucial technical foundation relies on the path behavior: if the starting point (t_s, h_s) lies high enough on Δ_δ , i.e., h_s large, then at some point the path enters a subset of Δ_δ that we call the *area of attraction* A_u of a change point $c_u \in C$, see Figure 2 (blue), and from this on it is systematically pushed towards the c_u .

For the process in Figure 1 MSCP yields estimates 145, 63 and 105 depicted in Figure 4, i.e., the number is correct, the smallest estimate at 63 is close to $c_1 = 65$ and the other two estimates even hit the true $c_2 = 105$ and $c_3 = 145$. MSCP is made available in the R-package `mscp` on CRAN Levajković and Messer (2021), which includes a summary and plotting routine while the latter created Figure 4: the top panel shows Δ_δ including S , and the paths constructed with detection orders indicated by integers (green). The middle panel gives the process and the means of the RVs in the detected sections (red), and the bottom shows the empirical variances therein (blue).

We strengthen three important upsides of MSCP: first, the method is non-parametric with weak distributional assumptions and thus allows to analyze a high variety of data. Robustness against additional changes in variance could be helpful in practice, as e.g., an increase in the mean might be accompanied with an increase in volatility. Second, the problem of window selection is overcome. Third, the gradual window adjustment improves the simultaneous detection of change points on multiple time scales and of different signal to noise ratios.

Estimation precision is corroborated by simulation studies investigating different change point scenarios and effect sizes. Various distributions are considered, including normal, gamma, Poisson and binomial, and their combinations. A comparison with state of the art methods reveals strong competitiveness of MSCP.

We mention that MSCP could be generalized generically, i.e., extended for the detection of other quantities than μ , e.g., higher moments, changes in slope, etc. For that, on the one hand

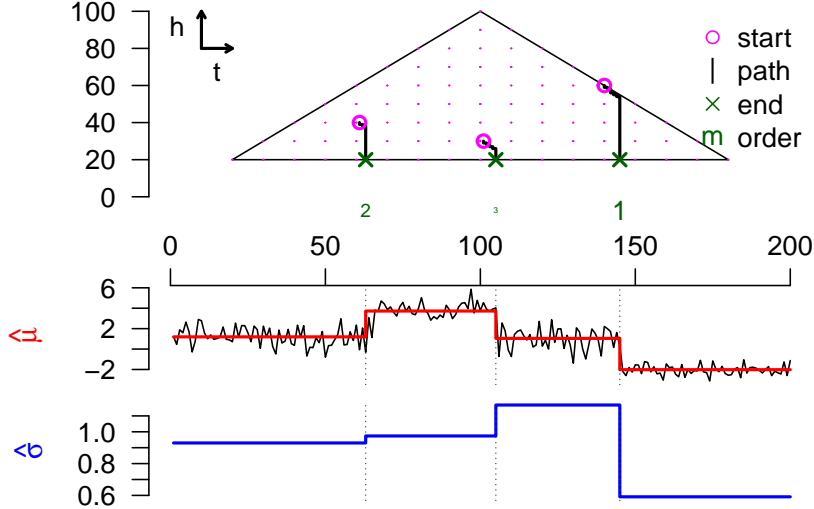


Figure 4: Plotting routine of the R-package `mscp`. It is $\hat{C} = \{63, 105, 145\}$.

both MOSUM $D_{t,h}$ in (1) and also model formulation needed adjustment, e.g., by considering a difference of empirical higher moments or estimated slopes. On the other hand, the intrinsic structure of MSCP, i.e., the successive construction of paths on Δ_δ would be maintained.

The paper is organized as follows: In Section 2 we specify the model, Δ_δ and $D_{t,h}$. In Section 3 we study properties of $(D_{t,h})_{(t,h) \in \Delta_\delta}$ which are used for change point detection. In Section 4 we construct the zigzag-path and show that it yields proper estimates. We introduce the set of starting points S , define MSCP, and state consistency. In Section 5 we discuss the tuning parameters (δ , S and the breaking criterion), present the simulations, and discuss a data example where MSCP segments a nucleotide sequence of a human genome. Proofs are given in the Appendix 6.

2 The change point model and MOSUM on the triangle

The model \mathcal{M} We fix $T \in \mathbb{N} \setminus \{0, 1\}$ and call $\{1, \dots, T\}$ the observation regime. We consider a subset $C \subset \{1, \dots, T-1\}$ of cardinality $|C|$ with ordered elements $c_1 < c_2 < \dots < c_{|C|}$. We call c_u the u -th change point and C the set of change points. C is treated fixed but unknown. Set $c_0 := 0$ and $c_{|C|+1} := T$, and the minimal distance of adjacent change points $\delta_C := \min_{u=1, \dots, |C|+1} (c_u - c_{u-1})$.

Let $(\Omega, \mathcal{A}, \mathbb{P})$ be a probability space and $p > 0$. We consider a triangular scheme: let $(Z_{u,i})_{u,i}$ for $u \in \{1, 2, \dots, |C|+1\}$ and $i = 1, 2, \dots$ be independent RVs in $\mathcal{L}^{2+p}(\Omega, \mathcal{A}, \mathbb{P})$ with $\mathbb{E}[Z_{u,i}] = 0$ and $\text{Var}(Z_{u,i}) = 1$, and let $(Z_{u,i})_{i=1,2,\dots}$ be an i.i.d. sequence for each u . Further let $\mu_1, \mu_2, \dots, \mu_{|C|+1} \in \mathbb{R}$ with $\mu_u \neq \mu_{u+1}$, and $\sigma_1^2, \sigma_2^2, \dots, \sigma_{|C|+1}^2$ positive. For $n \in \{1, 2, \dots\}$ set

$$X_i := \sum_{u=1}^{|C|+1} (\mu_u + \sigma_u Z_{u,i}) \cdot \mathbb{1}_{\{nc_{u-1}+1, \dots, nc_u\}}(i), \quad i \in \{1, 2, \dots, nT\}. \quad (2)$$

Dependence of X_i on n is suppressed for simplicity. The process $\mathbf{X} := (X_i)_{i=1,2,\dots,nT}$ has $|C|$ change points. In the section from $nc_{u-1} + 1$ to nc_u it has expectation μ_u and variance σ_u^2 , which are then changing to μ_{u+1} and σ_{u+1}^2 . The case $n = 1$ is considered the real-time

scenario. Throughout, asymptotics are studied letting $n \rightarrow \infty$, i.e., the observation regime and all change points increase linearly. Consequently, the relative change point location nc_u/nT is constant over n . The formulation of n in (2) facilitates to track scaling n^ϑ for different ϑ in the course of the article. Given T , the set of processes \mathbf{X} constitutes the model \mathcal{M} .

For all u , we set the first two moments $\mu_u^{(1)} := \mu_u$ and $\mu_u^{(2)} := \sigma_u^2 + \mu_u^2$ and the centered moments $\mu_u^{\{1\}} = 0$ and $\mu_u^{\{2\}} := \sigma_u^2$. If $C = \emptyset$, we set $\mu := \mu^{(1)} := \mu_1^{(1)}$, $\mu^{(2)} := \mu_1^{(2)}$ and $\sigma^2 := \sigma_1^2 := \mu_1^{\{2\}}$.

Local estimators and MOSUM For $(t, h) \in \Delta_\delta$, see Section 1, we consider indices interpreted a left and right window $I_\ell^{(n)} := \{\lfloor nt \rfloor - \lfloor nh \rfloor + 1, \dots, \lfloor nt \rfloor\}$ and $I_r^{(n)} := \{\lfloor nt \rfloor + 1, \dots, \lfloor nt \rfloor + \lfloor nh \rfloor\}$. We set local estimators for $\mu^{(k)}$ and $\mu^{\{k\}}$ for $j \in \{\ell, r\}$ via

$$\hat{\mu}_j^{\langle k \rangle} := \frac{1}{nh} \sum_{i \in I_j^{(n)}} X_i^k \quad \text{and} \quad \hat{\mu}_j^{\{k\}} := \frac{1}{nh} \sum_{i \in I_j^{(n)}} (X_i - \hat{\mu}_j^{\langle 1 \rangle})^k, \quad (3)$$

and abbreviate $\hat{\mu}_j := \hat{\mu}_j^{\langle 1 \rangle}$ and $\hat{\sigma}_j^2 := \hat{\mu}_j^{\{2\}}$. Dependence on t and h is suppressed to avoid overload. Then we define

$$D_{t,h}^{(n)} := \frac{\hat{\mu}_r - \hat{\mu}_\ell}{[(\hat{\sigma}_r^2 + \hat{\sigma}_\ell^2)/\lfloor nh \rfloor]^{1/2}}, \quad (4)$$

noting that $D_{t,h}^{(1)} = D_{t,h}$ from (1). We set $D_{t,h}^{(n)} := 0$ if the denominator vanishes. For each n the statistics are càdlàg step-functions in both directions t and h , with discontinuities in horizontal and vertical slices at values k/n , see Figure 5.

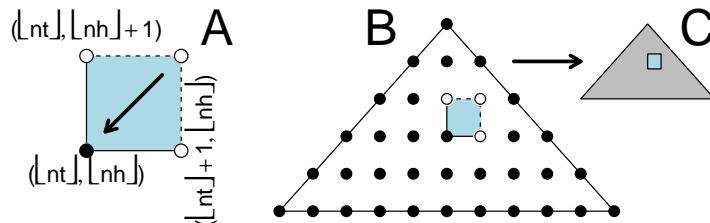


Figure 5: Process construction. The floor-functions (A) in $I_j^{(n)}$, $j \in \{\ell, r\}$ for both $\lfloor nt \rfloor$ and $\lfloor nh \rfloor$ appear within a factor- n -enlarged triangle (B), which is rescaled to Δ_δ (C).

Processes are considered in function space $(\mathcal{D}_{\mathbb{R}}[\mathcal{K}], \|\cdot\|_\infty)$. For a convex subset \mathcal{K} of \mathbb{R}^k with $k \in \{1, 2\}$ let $\mathcal{D}_{\mathbb{R}}[\mathcal{K}]$ denote the set of \mathbb{R} -valued functions on \mathcal{K} , which in case of $k = 1$ are càdlàg, and in case of $k = 2$ càdlàg with respect to each component when the other component is fixed. $\mathcal{D}_{\mathbb{R}}[\mathcal{K}]$ is endowed with uniform distance $\|\cdot\|_\infty$. As asymptotics yield almost surely (a.s.) continuous limits, there is no need to evoke Skorokhod topology.

3 Asymptotics of the estimators

Strong consistency We state strong convergence of the estimators. We define their limits pointwise for $(t, h) \in \Delta_\delta$. They are weightings of the theoretical moments depending on the change point locations relative to the window. Consider the left window $(t-h, t]$ and assume that the change points that are overlapped are $C_\ell \subset C$, i.e., we find $t-h < c_{\ell,1} < c_{\ell,2} < \dots < c_{\ell,|C_\ell|} \leq t$, and $c_{\ell,u}$ denotes the u -th smallest change point in C_ℓ . Set $c_{\ell,0} := t-h$ and

$c_{\ell, |C_\ell|+1} := t$. For $u = 1, 2, \dots, |C_\ell| + 1$ set the distance $d_{\ell, u} := c_{\ell, u} - c_{\ell, u-1}$ between adjacent change points. The moments related to these sections are abbreviated by $\mu_{\ell, u}^{(k)}$ and $\sigma_{\ell, u}^2$, see Figure 6 left. From this we set

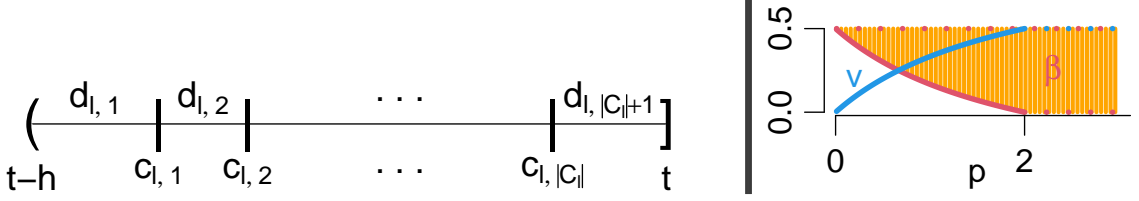


Figure 6: Left: schematic representation of the left window overlapping $|C_\ell|$ change points. Right: Parameters v and β depending on p .

$$\tilde{\mu}_\ell^{(k)} := \sum_{u=1}^{|C_\ell|+1} \frac{d_{\ell, u}}{h} \cdot \mu_{\ell, u}^{(k)} \quad \text{and} \quad \tilde{\sigma}_\ell^2 := \sum_{u=1}^{|C_\ell|+1} \frac{d_{\ell, u}}{h} \cdot [\sigma_{\ell, u}^2 + (\tilde{\mu}_\ell - \mu_{\ell, u})^2], \quad (5)$$

with $\tilde{\mu}_\ell := \tilde{\mu}_\ell^{(1)}$. The limits weight the moments with the time $d_{\ell, u}$ spent in a section relative to the window length $h = \sum_u d_{\ell, u}$. Further we set

$$\tilde{\sigma}_\ell^2 := \sum_{u=1}^{|C_\ell|+1} \frac{d_{\ell, u}}{h} \cdot \sigma_{\ell, u}^2, \quad \text{and} \quad e_\ell^2 := \sum_{u=1}^{|C_\ell|+1} \frac{d_{\ell, u}}{h} (\tilde{\mu}_\ell - \mu_{\ell, u})^2, \quad (6)$$

and note that $\tilde{\sigma}_\ell^2 = \tilde{\sigma}_\ell^2 + e_\ell^2$, i.e., $\tilde{\sigma}_\ell^2$ weights not only the variances $\sigma_{\ell, u}^2$ as in $\tilde{\sigma}_\ell^2$, but also the additional error term e_ℓ^2 . The error accounts for the violation of change points in the calculation of the mean in the computation of the empirical variance – the mean is calculated from all data in the windows ‘violating’ unknown change points. It is $e_\ell^2 \geq 0$. If no change points are overlapped $C_\ell = \emptyset$, then the limits simplify to single theoretical moments $\tilde{\mu}_\ell^{(k)} = \mu_{\ell, 1}^{(k)}$ and $\tilde{\sigma}_\ell^2 = \tilde{\sigma}_\ell^2 = \sigma_{\ell, 1}^2$ and also $e_\ell^2 = 0$. Analogously we define the limits $\tilde{\mu}_r^{(k)}$ and $\tilde{\sigma}_r^2$ for the right window $(t, t+h]$ by considering the change points C_r whose ordered elements $c_{r, u}$ fulfill $t < c_{r, 1} < c_{r, 2} < \dots < c_{r, |C_r|} \leq t+h$. If $C = \emptyset$, then for all $(t, h) \in \Delta_\delta$ we obtain the population parameters $\tilde{\mu}_j = \mu$, $\tilde{\sigma}_j^2 = \sigma^2$ etc. In the following we state strong consistency of the estimators.

Lemma 3.1. *Let $\mathbf{X} \in \mathcal{M}$. For $j \in \{\ell, r\}$ it holds in $(\mathcal{D}_{\mathbb{R}}[\Delta_\delta], \|\cdot\|_\infty)$ a.s. as $n \rightarrow \infty$*

$$n^v \cdot (\hat{\mu}_j^{(k)} - \tilde{\mu}_j^{(k)})_{(t, h)} \longrightarrow (0)_{(t, h)} \text{ for } v \in \begin{cases} (-\infty, 1/2), & \text{if } k = 1 \\ (-\infty, 1/2) \cap (-\infty, p/(p+2)], & \text{if } k = 2, \end{cases}$$

and $n^v \cdot (\hat{\sigma}_j^2 - \tilde{\sigma}_j^2)_{(t, h)} \rightarrow (0)_{(t, h)}$ with $v \in (-\infty, 1/2) \cap (-\infty, p/(p+2)]$.

The result follows from the Marcinkiewicz-Zygmund SLLN, noting that $\mathbb{E}[|X_i|^{2+p}] < \infty$. See v in Figure 6 right: for $k = 1$ we cannot reach $1/2$ noting CLT and LIL, and for $k = 2$ the rate improves with the existence of higher moments via p , but only for $p < 2$ while $p/(2+p) < 1/2$, i.e., $p \geq 2$ brings no improvement. Any rate for $k = 2$ is valid for $k = 1$.

The systematic component of $(D_{t, h}^{(n)})_{(t, h) \in \Delta_\delta}$ is the centering $(d_{t, h}^{(n)})_{(t, h) \in \Delta_\delta}$ given by

$$d_{t, h}^{(n)} := \frac{\tilde{\mu}_r - \tilde{\mu}_\ell}{[(\tilde{\sigma}_r^2 + \tilde{\sigma}_\ell^2)/[nh]]^{1/2}}. \quad (7)$$

We note that $n^{-1/2} \cdot d_{t,h}^{(n)} = d_{t,h}^{(1)}$ and conclude from Lemma 3.1

Corollary 3.2. *Let $\mathbf{X} \in \mathcal{M}$. For $v \in (-\infty, 1/2) \cap (-\infty, p/(p+2)]$ it holds in $(\mathcal{D}_{\mathbb{R}}[\Delta_\delta], \|\cdot\|_\infty)$ a.s. as $n \rightarrow \infty$*

$$n^v \cdot \left(\frac{1}{\sqrt{n}} D_{t,h}^{(n)} - d_{t,h}^{(1)} \right)_{(t,h)} \rightarrow (0)_{(t,h)}.$$

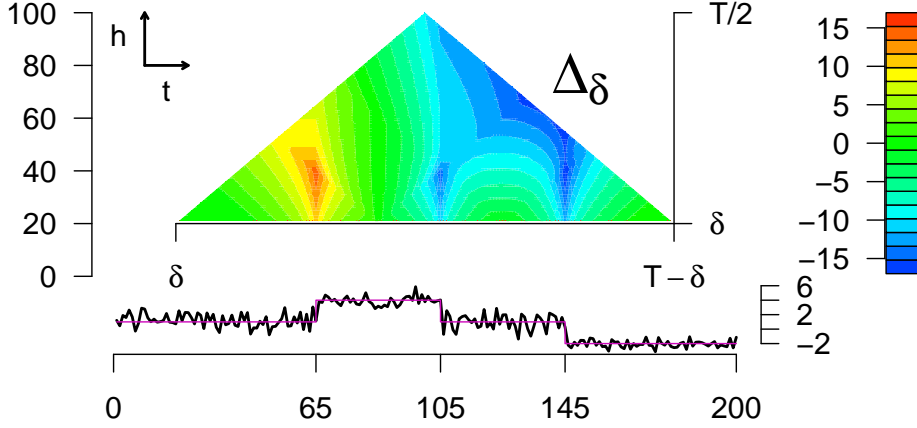


Figure 7: $d_{t,h}^{(1)}$ relating to $D_{t,h}^{(1)}$ from Figure 1.

Figure 7 shows $d_{t,h}^{(1)}$ relating to $D_{t,h}^{(1)}$. It has an analogous shape, but smoother as noise is canceled out. We will construct the zigzag-path from $D_{t,h}^{(n)}$ and deduce properties from a non-random path based on $d_{t,h}^{(n)}$.

Considering a single change point We describe $(d_{t,h}^{(n)})_t$ for fixed h as a function of t . Let $c_u \in C$. We assume h small such that only c_u is overlapped by the double-window when it is near c_u . We formalize the shape of $(d_{t,h}^{(n)})_t$ in Lemma 3.3, which will be used to show that the zigzag-path is pushed towards c_u when it comes close to it.

If $c_{u+1} - c_u \geq h$ and $c_u - c_{u-1} > h$, then set $\tau_h := [c_{u-1} + h, c_{u+1} - h)$, else set $\tau_h := \emptyset$. For h small it is $\tau_h \neq \emptyset$. In this case $(d_{t,h}^{(n)})_{t \in \tau_h}$ is continuous, it vanishes if $|t - c_u| \geq h$ because no $c \in C$ is overlapped, and it systematically deviates from zero if $|t - c_u| < h$ with extreme value $t = c_u$, see Figure 8E in which the blue and red lines indicate a uniform bound for the derivative. We set $v_{t,h} := [(\tilde{\sigma}_r^2 + \tilde{\sigma}_\ell^2) / (\tilde{\sigma}_r^2 + \tilde{\sigma}_\ell^2)]^{1/2}$, recalling $\tilde{\sigma}_j^2 = \tilde{\sigma}_j^2 + e_j^2$, see (5) and (6), and denote \wedge the minimum and \vee the maximum.

Lemma 3.3. *Let $\mathbf{X} \in \mathcal{M}$, $c_u \in C$ and h be fixed such that $\tau_h \neq \emptyset$. Then both $(d_{t,h}^{(n)})_{t \in \tau_h}$ and $(v_{t,h} \cdot d_{t,h}^{(n)})_{t \in \tau_h}$ are continuous and zero for $t \in \tau_h \setminus [c_u - h, c_u + h)$. For $t \in [c_u - h, c_u + h)$, four cases are differentiated regarding $d_{t,h}^{(n)}$: for $\mu_{u+1} > \mu_u$ we find that*

$$d_{t,h}^{(n)} \text{ is } \begin{cases} \text{strictly increasing for } t \in [c_u - h, c_u], \\ \text{strictly decreasing for } t \in (c_u, c_u + h]. \end{cases} \quad (8)$$

For $\mu_{u+1} < \mu_u$ it is 'increasing' and 'decreasing' replaced. Further, for $t \in (c_u - h, c_u) \cup$

$(c_u, c_u + h)$ it is

$$\sqrt{nh} \cdot \kappa_a \leq \left| \frac{\partial}{\partial t} d_{t,h}^{(n)} \right| \leq \sqrt{nh} \cdot \kappa_b, \quad (9)$$

with constants

$$\begin{aligned} \kappa_a &:= |\mu_{u+1} - \mu_u| \cdot \frac{2(\sigma_{u+1}^2 \wedge \sigma_u^2)}{[2(\sigma_{u+1}^2 \vee \sigma_u^2) + (\mu_{u+1} - \mu_u)^2/4]^{3/2}}, \\ \kappa_b &:= |\mu_{u+1} - \mu_u| \cdot \frac{2(\sigma_{u+1}^2 \vee \sigma_u^2) + (\mu_{u+1} - \mu_u)^2}{[2(\sigma_{u+1}^2 \wedge \sigma_u^2)]^{3/2}}. \end{aligned}$$

Regarding $v_{t,h} \cdot d_{t,h}^{(n)}$ six cases are differentiated: for $\mu_{u+1} > \mu_u$ and

$$\begin{aligned} \sigma_{u+1}^2 = \sigma_u^2 : \quad v_{t,h} \cdot d_{t,h}^{(n)} \quad \text{is} & \begin{cases} \text{linear and strictly increasing for } t \in [c_u - h, c_u], \\ \text{linear and strictly decreasing for } t \in (c_u, c_u + h]. \end{cases} \\ \sigma_{u+1}^2 > \sigma_u^2 : \quad v_{t,h} \cdot d_{t,h}^{(n)} \quad \text{is} & \begin{cases} \text{strictly concave and strictly increasing for } t \in [c_u - h, c_u], \\ \text{strictly convex and strictly decreasing for } t \in (c_u, c_u + h]. \end{cases} \\ \sigma_{u+1}^2 < \sigma_u^2 : \quad v_{t,h} \cdot d_{t,h}^{(n)} \quad \text{is} & \begin{cases} \text{strictly convex and strictly increasing for } t \in [c_u - h, c_u], \\ \text{strictly concave and strictly decreasing for } t \in (c_u, c_u + h]. \end{cases} \end{aligned}$$

For $\mu_{u+1} < \mu_u$, the expressions hold true, but with 'convex' and 'concave' as well as 'increasing' and 'decreasing' replaced. It is $v_{t,h} \cdot |d_{t,h}^{(n)}| \geq |d_{t,h}^{(n)}|$ with equality at $t = c_u$.

Both $(v_{t,h} \cdot d_{t,h}^{(n)})_t$ and $(d_{t,h}^{(n)})_t$ are depicted in Figure 8D and E.

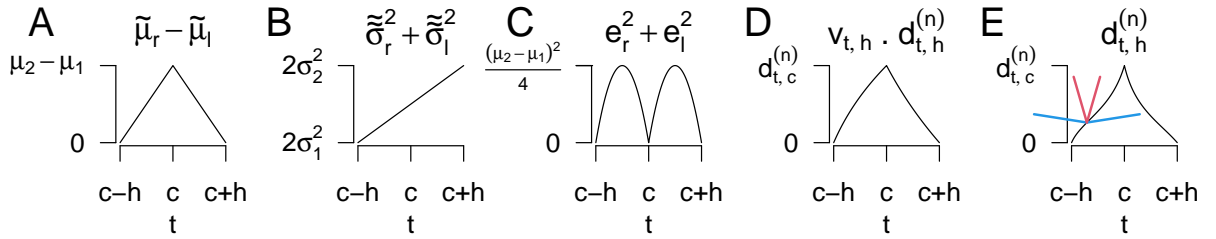


Figure 8: Construction of $(d_{t,h}^{(n)})_{t \in \tau_h}$ (for $c = c_1$). A: $\tilde{\mu}_r - \tilde{\mu}_\ell$, B: $\tilde{\sigma}_r^2 + \tilde{\sigma}_\ell^2$, C: $e_r^2 + e_\ell^2$, D: $v_{t,h} \cdot d_{t,h}^{(n)}$, E: $d_{t,h}^{(n)}$ and lines with slopes $\mp(nh)^{1/2} \cdot \kappa_a$ (blue) and $\mp(nh)^{1/2} \cdot \kappa_b$ (red).

Figure 8 shows the statistics that factor into $(d_{t,h}^{(n)})_{t \in \tau_h}$. It is $\mu_2 > \mu_1$ and $\sigma_2^2 > \mu_2^2$. The function $\tilde{\mu}_r - \tilde{\mu}_\ell$ has the shape of a hat (A). It is positive as $\mu_2 > \mu_1$. The function $\tilde{\sigma}_r^2 + \tilde{\sigma}_\ell^2$ is linear (B). It is increasing as $\sigma_2^2 > \sigma_1^2$. The error $e_r^2 + e_\ell^2$ describes two parabolas and vanishes outside the h -neighborhood of $c := c_u$ and also at c (C). The error is maximal at $c \mp h/2$ which are the points where either the right or the left window is divided in half and thus equally sharing the left and right population. Panel D shows $v_{t,h} \cdot d_{t,h}^{(n)}$ which is $(nh)^{1/2}$ times (A) divided by the square-root of (B). It is non-negative as $\mu_2 > \mu_1$ and concave on $[c - h, c]$ and convex on $(c, c + h]$ as $\sigma_2^2 > \sigma_1^2$. Panel D shows $d_{t,h}^{(n)}$ which is $(nh)^{1/2}$ times (A) divided by the square-root of the sum of (B) and (C). As $\mu_2 > \mu_1$, it is strictly increasing in $[c - h, c]$ and strictly decreasing on $(c, c + h]$. It is $v_{t,h} \cdot d_{t,h}^{(n)} \geq d_{t,h}^{(n)}$, as $v_{t,h} \geq 1$. Note that in Lemma 3.3 it is $0 < \kappa_a < \kappa_b < \infty$, and κ_a, κ_b depend only on the population parameters, such that the bounds

for the derivative in (9) depend on h but not on t . The upper bound $(nh)^{1/2} \cdot \kappa_b$ is a Lipschitz constant for $(d_{t,h}^{(n)})_t$. Figure 8E shows lines with slopes $\mp(nh)^{1/2} \cdot \kappa_a$ (blue) and $\mp(nh)^{1/2} \cdot \kappa_b$ (red), i.e., the slope of $(d_{t,h}^{(n)})_t$ varies in between for all $t \in (c_u - h, c_u) \cup (c_u, c_u + h)$.

Weak convergence We state weak convergence of $(D_{t,h}^{(n)})_{(t,h) \in \Delta_\delta}$ if $C = \emptyset$. Let $(W_t)_{t \geq 0}$ be a standard Brownian motion. Then define $(L_{t,h})_{(t,h) \in \Delta_\delta}$ via $L_{t,h} := (2h)^{-1/2} \cdot [(W_{t+h} - W_t) - (W_t - W_{t-h})]$. The process $(L_{t,h})_{(t,h)}$ is continuous with $L_{t,h} \sim N(0, 1)$.

Proposition 3.4. *Let $\mathbf{X} \in \mathcal{M}$ with $C = \emptyset$. In $(\mathcal{D}_{\mathbb{R}}[\Delta_\delta], \|\cdot\|_\infty)$ it holds as $n \rightarrow \infty$ that $(D_{t,h}^{(n)})_{(t,h)} \xrightarrow{d} (L_{t,h})_{(t,h)}$.*

$L_{t,h}$ preserves the double-window structure of $D_{t,h}^{(n)}$, zero mean aligns with $C = \emptyset$ and unit variance results from scaling of $D_{t,h}^{(n)}$. The proof applies Donsker's theorem.

We mention that the upper limit theorems could be extended to dependent data structures, for which in $D_{t,h}^{(n)}$ from (4) the variance estimator first needed to address that dependence. As a consequence, MSCP formulated in the following section would apply to those scenarios as well. For recent developments of change point detection methods w.r.t. dependent data see e.g., (Baranowski et al., 2019a; Dette et al., 2020), supplement (Fryzlewicz, 2018a) of (Fryzlewicz, 2018b), or the overview article (Aue and Horváth, 2013).

4 Change point detection via MSCP

Segmentation of the triangle We specify regions of Δ_δ . Each $c_u \in C$ has an area of attraction $A_u := \{(t, h) \in \Delta_\delta : c_{u-1} \leq t - h < c_u \leq t + h < c_{u+1}\}$, see Figure 2 (blue). For all $(t, h) \in A_u$ the associated double window overlaps c_u but no other change point. It is $|d_{t,h}^{(n)}| > 0$ for $(t, h) \in A_u$. We show that path that starts in A_u is systematically pushed towards c_u , such that its endpoint becomes a proper estimate for c_u . We also set $B_u := \{(t, h) \in A_u : |t - c_u| \leq h - \delta + 1\}$, for whose elements we find the 't-distance' to c_u smaller than the 'h-distance' (plus 1) to the bottom of Δ_δ . For any $t_0 \in [\delta, T - \delta]$ we define its cone $K_{t_0} := \{(t, h) \in \Delta_\delta : t - h < t_0 \leq t + h\}$. The cones K_{c_u} of the $c_u \in C$ are shown in Figure 2 (orange). K_{c_u} consists of all $(t, h) \in \Delta_\delta$ for which the double window overlaps c_u and possibly neighboring change points. It holds $B_u \subset A_u \subset K_{c_u} \subset \Delta_\delta$. Finally, we consider the remainder $R := \Delta_\delta \setminus \bigcup_{u=1}^{|C|} K_{c_u}$, that consists of $(t, h) \in \Delta_\delta$ for which no c_u is overlapped by the double window, such that $d_{t,h}^{(n)} = 0$ for all $(t, h) \in R$. In Figure 2, R consists of four subtriangles of Δ_δ as there are three change points involved.

The zigzag-downpath We construct a path on $\Delta_\delta \cap \mathbb{N}^2$ w.r.t. either $D_{t,h}^{(n)}$ or $d_{t,h}^{(n)}$.

Algorithm 4.1. (*zigzag-downpath*)

Input: $\mathbf{X} \in \mathcal{M}$ and a starting value $(t_s, h_s) \in \Delta_\delta \cap \mathbb{N}^2$. Set $f_{t,h}^{(n)} \in \{d_{t,h}^{(n)}, D_{t,h}^{(n)}\}$.

Construction: set $t_s^{(n)}(0) := \min \left(\operatorname{argmax}_{t \in \{t_s-1, t_s, t_s+1\} \cap \Delta_\delta} n^{-1/2} \cdot |f_{t,h_s}^{(n)}| \right)$. For $k = 1, 2, \dots, h_s - \delta$ iteratively define

$$t_s^{(n)}(k) := \min \left(\operatorname{argmax}_{t \in \{t_s^{(n)}(k-1)-1, t_s^{(n)}(k-1), t_s^{(n)}(k-1)+1\}} n^{-1/2} \cdot |f_{t, h_s-k}^{(n)}| \right). \quad (10)$$

Output: the zigzag downpath $(t_s^{(n)}(k), h_s - k)_{k=0,1,2,\dots,h_s-\delta}$.

In $t_s^{(n)}(0)$ we start with choosing the maximizer among $\{t_s - 1, t_s, t_s + 1\} \cap \Delta_\delta$ and the restriction to Δ_δ yields well-definedness if (t_s, h_s) lies on its edge. The minimum in $t_s^{(n)}(k)$ ensures uniqueness. For $f_{t,h}^{(n)} = D_{t,h}^{(n)}$ the maximum is necessarily a.s. unique in case the RVs of \mathbf{X} lack point masses. We abbreviate the end $t_e^{(n)} := t_s^{(n)}(h_s - \delta)$. In order to differentiate the paths we write

$$t_s^{(n)}(k) =: \begin{cases} t_s(k), & \text{if } f_{t,h}^{(n)} = d_{t,h}^{(n)}, \\ \hat{t}_s^{(n)}(k), & \text{if } f_{t,h}^{(n)} = D_{t,h}^{(n)}, \end{cases} \quad (11)$$

and accordingly t_e and $\hat{t}_e^{(n)}$, noting that for $f_{t,h}^{(n)} = d_{t,h}^{(n)}$ the path is independent of n , as $n^{-1/2} \cdot |d_{t,h}^{(n)}| = |d_{t,h}^{(1)}|$.

Path behavior w.r.t $d_{t,h}^{(n)}$ A path starting in A_u systematically tends towards c_u :

Lemma 4.2. *Let $\mathbf{X} \in \mathcal{M}$, $c_u \in C$ and $f_{t,h}^{(n)} = d_{t,h}^{(n)}$. If $(t_s, h_s) \in A_u$, then for all $k \in \{1, 2, \dots, h_s - \delta\}$ it holds*

$$t_s(k) - t_s(k-1) = \begin{cases} 0, & \text{if } |t_s - c_u| \leq k, \\ 1, & \text{if } t_s < c_u - k, \\ -1, & \text{if } t_s > c_u + k, \end{cases} \quad (12)$$

If $(t_s, h_s) \in B_u$, then $t_e = c_u$. If $(t_s, h_s) \in A_u \setminus B_u$, then $|t_e - c_u| \leq \delta - 1$.

Lemma 4.2 states that in each step $t_s(k)$ either increases by unity if $t_s < c_u$ or it decreases by unity if $t_s > c_u$, and if it reaches c_u then it stays. Thus, the path $(t_s(k), h_s - k)_k$ is perfectly zigzagging towards the vertical line at c_u . If it reaches this line then it moves vertically downwards to the lower edge of Δ_δ , i.e., $t_e = c_u$. The proof exploits the shape of $(d_{t,h}^{(n)})_t$ stated in Lemma 3.3.

Path behavior w.r.t $D_{t,h}^{(n)}$ Regarding $D_{t,h}^{(n)}$, a path starting in A_u converges towards the path w.r.t. $d_{t,h}^{(n)}$:

Proposition 4.3. *Let $\mathbf{X} \in \mathcal{M}$, $c_u \in C$ and $f_{t,h}^{(n)} = D_{t,h}^{(n)}$. Let $(t_s, h_s) \in A_u$, then for all $k \in \{0, 1, 2, \dots, h_s - \delta\}$ it holds that $\hat{t}_s^{(n)}(k) \rightarrow t_s(k)$ a.s. as $n \rightarrow \infty$ for all k , while $t_s(k)$ is given in (12).*

Consequently, starting in A_u yields detection of c_u up to a distance of $\delta - 1$. More precisely, for $(t_s, h_s) \in B_u$ we find $\lim_{n \rightarrow \infty} \hat{t}_e^{(n)} = c_u$ a.s., and for $(t_s, h_s) \in A_u \setminus B_u$ it is $\lim_{n \rightarrow \infty} |\hat{t}_e^{(n)} - c_u| \leq \delta - 1$ a.s. The proof exploits proximity of $D_{t,h}^{(n)}$ and $d_{t,h}^{(n)}$.

Starting points We call a set $S \subset \mathbb{N}^2 \cap \Delta_\delta$ a sufficient set of starting points if $S \cap A_u \neq \emptyset$ for all $u = 1, \dots, |C|$, i.e., for all $c_u \in C$ there lies a starting point in A_u . For a mesh size $g \in \mathbb{N}$ set a grid $S_g := (g \cdot \mathbb{N}^2) \cap \Delta_\delta$, see Figure 3A (pink dots).

Lemma 4.4. *Let $\mathbf{X} \in \mathcal{M}$ and $\delta < \lfloor \delta_C/2 \rfloor$. A grid S_g is sufficient if $g \leq \lfloor \delta_C/2 \rfloor$.*

The proof applies geometry. When a path enters A_u , then c_u is detected up to a distance of $\delta - 1$, see Proposition 4.3. Thus, when considering all paths starting in S , then all $c \in C$ will be detected. We need to avoid multiple detections of any c as well as false positives.

Change point detection Set $\min \emptyset := \infty$, and for a set F denote $U(F)$ a uniformly sampled element.

Algorithm 4.5. (MSCP)

Input: $\mathbf{X} \in \mathcal{M}$, a set of starting values S ,

and constants $\kappa > 0$, and $\beta \in [1/2 - v, 1/2)$ for $v \in (0, 1/2) \cap (0, p/(p+2)]$.

Initialize: counter $m = 1$, estimates $\hat{C}_m^{(n)} = \emptyset$ and starting values $S_m^{(n)} = S$.

While $S \neq \emptyset$, *loop:*

1. Choose the starting value $(\hat{t}_{s,m}^{(n)}, \hat{h}_{s,m}^{(n)}) := U(\operatorname{argmax}_{(t,h) \in S_m^{(n)}} [(nh)^{-1/2} \cdot |D_{t,h}^{(n)}|])$.
2. Run the zigzag-path w.r.t. $(\hat{t}_{s,m}^{(n)}, \hat{h}_{s,m}^{(n)})$ and $f_{t,h}^{(n)} = D_{t,h}^{(n)}$,
call the path $(\hat{t}_{s,m}^{(n)}(k), \hat{h}_{s,m}^{(n)} - k)_{k=0,1,2,\dots,\hat{h}_{s,m}^{(n)} - \delta}$ and the endpoint $(\hat{t}_{e,m}^{(n)}, \delta)$,
and compute the minimal distance $\mathcal{D}_m^{(n)} := \min\{|\hat{t}_{e,m}^{(n)} - \hat{c}^{(n)}| : \hat{c}^{(n)} \in \hat{C}^{(n)}\}$.
3. Check for multiple detections (3a.) and false positives (3b.)
 - 3a. If $\mathcal{D}_m^{(n)} \leq 2(\delta - 1)$, then set $S_m^{(n)} := S_m^{(n)} \setminus K_{\hat{t}_{e,m}^{(n)}}^{(n)}$ and Goto 1.
 - 3b. If $\max_{k=0,1,\dots,\hat{h}_{s,m}^{(n)} - \delta} |D_{\hat{t}_{s,m}^{(n)}(k), \hat{h}_{s,m}^{(n)} - k}^{(n)}| < \kappa \cdot n^\beta$, then break the loop.
 - [3c. Optional: If $\mathcal{D}_m^{(n)} < \delta_C - 2(\delta - 1)$, then break the loop. (Needs input δ_C .)]
4. Update $m = m + 1$, then set $\hat{C}_m^{(n)} = \hat{C}_{m-1}^{(n)} \cup \{\hat{t}_{e,m-1}^{(n)}\}$ and $S_m^{(n)} = S_{m-1}^{(n)} \setminus K_{\hat{t}_{e,m-1}^{(n)}}^{(n)}$,
and Goto 1.

Output: $\hat{C}^{(n)} := \hat{C}_m^{(n)}$.

The parameters κ and β yield a threshold $\kappa \cdot n^\beta$ (in 3b.), and if chosen large then this supports breaking the algorithm. Recall $E[|X_1|^{2+p}] < \infty$. β is related to p via v , see Figure 6 right. Small p forces β close to $1/2$ and a larger p allows for smaller β . The parameter β is redundant if $n = 1$. In 1., the maximum is a.s. unique if the RVs of \mathbf{X} do not have point masses. In general, uniform sampling yields well-definedness. It is $\mathcal{D}_1^{(n)} = \infty$.

Algorithm 4.5 (MSCP) is depicted in Figure 3. Successively, C is estimated. We comment on the steps.

- 1.: Among all current starting points the one maximizing $(nh)^{-1/2} \cdot |D_{t,h}^{(n)}|$ is chosen, uniformly in case of non-uniqueness. This ensures the starting point to lie outside the remainder R , a.s. for n large, in case of remaining undetected change points.
- 2.: The zigzag-path is constructed and $\hat{t}_{e,m}^{(n)}$ functions as a change point candidate. The minimal distance $\mathcal{D}_m^{(n)}$ of $\hat{t}_{e,m}^{(n)}$ and all previous estimates is computed.
- 3.: Two aspects are addressed:
 - 3a.: 'Avoiding multiple detections': if $\mathcal{D}_m^{(n)} \leq 2(\delta - 1)$, then $\hat{t}_{e,m}^{(n)}$ is rejected, all starting points from its cone are cut, and estimation restarts. The rationale is that if the paths of both $\hat{t}_{e,m}^{(n)}$ and the closest estimate passed A_u , then they also systematically led to c_u up to $\delta - 1$. Hence, rejection of such $\hat{t}_{e,m}^{(n)}$ avoids multiple detections.

3b.: 'Avoiding false positives': if $\hat{t}_{e,m}^{(n)}$ was not rejected in 3a., then decision is made of whether the loop breaks. If the objection function takes extreme values on the zigzag-path, then this supports $\hat{t}_{e,m}^{(n)}$ to indicate an $c_u \in C$, and thus it is accepted in 4., and the next iteration starts after the cone of $\hat{t}_{e,m}^{(n)}$ is cut to avoid further detections of c_u .

Note that we allow an error up to $\delta - 1$, and if the distance of $\hat{t}_{e,m}^{(n)}$ to c_u is positive, then a slightly shifted cone was cut. This gives rise for 3a. at first. Also note that if all $c \in C$ are detected and near cones are cut (again mentioning 3a.), then what is eventually left over is the remainder R . Thus, on the next path the objection function will no longer take extreme values which support breaking in 3b., and the previous estimates are returned. Finally note that the breaking criterion 3c. applies if the minimal distance between change points was exceeded, also accounting for estimation precision only up to $\delta - 1$. Asymptotically, this will not occur, so 3c. is obsolete for theoretical consistency, but may be used in practice.

We denote $\hat{c}_u^{(n)}$ the u -th smallest element of $\hat{C}^{(n)}$. For well-definedness, if $|\hat{C}^{(n)}| < |C|$ set $\hat{c}_u^{(n)} := 0$ for all $u = |\hat{C}^{(n)}| + 1, \dots, |C|$. The algorithm succeeds:

Theorem 4.6. *Let $\lfloor \delta_C/2 \rfloor > \delta$. In Algorithm 4.5 let the input S be sufficient. Then for the output $\hat{C}^{(n)}$ it holds a.s. as $n \rightarrow \infty$ that*

$$|\hat{C}^{(n)}| \longrightarrow |C| \quad \text{and} \quad \limsup_{n \rightarrow \infty} |\hat{c}_u^{(n)} - c_u| \leq \delta - 1 \quad \text{for all } u = 1, \dots, |C|.$$

Location estimation is correct up to $\delta - 1$. The choice $\delta = 1$ states strong consistency. Recall that $\lfloor \delta_C/2 \rfloor > \delta$ is needed for sufficiency of $S = S_g$ in Lemma 4.4. Also it implies $\delta_C > 2(\delta - 1)$, i.e., neighboring change points should be separated by more than the worst errors of their estimators. The proof applies Proposition 4.3 for the estimation of C , and Corollary 3.2 for correct breaking.

5 Practical aspects

Parameter choice We give recommendations for the choice of S , κ and δ in practice, where $n = 1$. Then, the threshold is $\kappa \cdot n^\beta = \kappa$, i.e., β is redundant.

1. Choice of κ : κ can be chosen as the rejection threshold of a test for $H_0 : C = \emptyset$: For H_0 Proposition 3.4 implies weak convergence of $\sup_{t,h \in \Delta_\delta} |D_{t,h}^{(n)}| \rightarrow \sup_{(t,h) \in \Delta_\delta} |L_{(t,h)}|$ as $n \rightarrow \infty$, and we choose κ as the $(1 - \alpha)$ -quantile of the limit distribution (e.g., significance level $\alpha = 0.01$), which can be derived in simulations, compare e.g., Messer et al. (2014). If $|\hat{C}^{(1)}| > 0$, then H_0 is rejected at level $\leq \alpha$, as the maximum w.r.t. a path is bounded by the supreme over Δ_δ .
2. Choice of S : Lemma 4.4 states sufficiency of $S = S_g$ if $g \leq \lfloor \delta_C/2 \rfloor$ (in case $\delta < \lfloor \delta_C/2 \rfloor$). Thus, if δ_C is known it is reasonable to choose $g = \lfloor \delta_C/2 \rfloor$ as g large reduces computational complexity. If δ_C is unknown, we set $g = \delta$ or even smaller if computational complexity allows for.
3. Choice of δ : We recommend $\delta = 20$: by construction, asymptotic considerations imply an increase of the double windows. For $n \rightarrow \infty$, weakly $D_{t,h}^{(n)} \rightarrow L_{t,h} \sim N(0, 1)$ for all

$(t, h) \in \Delta_\delta$, but for $n = 1$ small h means less observations and the approximation via $N(0, 1)$ is harder to justify. Practically, for tiny h there is high variability in $\hat{\mu}_j$ and $\hat{\sigma}_j^2$ and thus $D_{t,h}^{(1)}$ is likely to take extreme values even if no change is involved, resulting in false positives. Thus, δ should be bounded from below. Figure 9 shows simulations for the probability that $\mathbb{P}(|\hat{C}^{(1)}| > 0)$ if $C = \emptyset$ (rejection probability under H_0), for both $\alpha = 0.05$ and $\alpha = 0.01$, depending on δ . Over a variety of distributions, including normal, exponential, gamma, binomial and Poisson, for $\delta \geq 20$ the α -level is kept throughout.

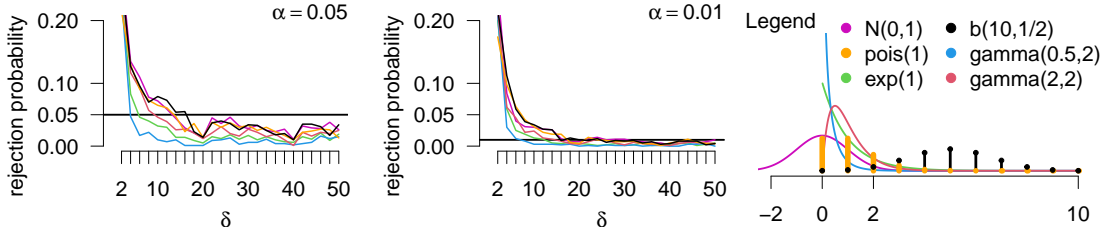


Figure 9: Rejection probability under $C = \emptyset$ (1000 simulations) depending on $\delta \in \{2, 4, \dots, 50\}$. $T = 1000$, left: $\alpha = 5\%$, right: $\alpha = 1\%$. Six distributions color coded: $N(0, 1)$ (magenta), $Pois(1)$ (orange), $exp(1)$ (green), $b(10, 1/2)$ (black), $gamma(0.5, 2)$ (blue) and $gamma(2, 2)$ (red). Right: Legend.

In the following we use $\delta = g = 20$ and κ is derived in simulations for $\alpha = 0.01$.

Simulation studies We evaluate the performance of MSCP in simulation studies. Throughout it is $T = 1000$ and $|C| = 5$. We consider different scenarios of locations $c_u \in C$ and parameters μ_u and σ_u , given in Table 1. Scenarios 1–3 differ in C : in 1 it is $c_{u+1} - c_u = 200$, and in 2 it is $c_{u+1} - c_u = 100$ throughout, and 3 describes a multiscale setup where $c_1 = 200$ is well separated and for the others it is $c_{u+1} - c_u = 50$. For each choice of C we then consider different effects by altering both changes in μ_u and in σ_u . E.g., 1a states certain μ_u which are halved in 1c. Also, in 1a it is $\sigma_u = 1$ constant, while in 1b the σ_u alter between 1 and 2. For each scenario we consider different distributions: A. $N(\mu, \sigma^2)$ (normal), B. $gamma(s, \lambda)$ (gamma), C. $Poi(\lambda)$ (Poisson), D. $b(10, p)$ (binomial, $n = 10$ fix), and E. is a combination of the previous that changes between the six sections using A.,B.,C.,D.,A.,B. (mix). Note that for $Poi(\lambda)$ and $b(10, p)$ the formulation of σ_u can be disregarded as it follows from μ_u , and also if distributions coincide due to equality of μ_u as e.g., in 1a and 1b, they are presented only once.

For each scenario we run 1000 simulations, i.e., there are $1000 \cdot |C| = 5000$ change points in total. W.r.t. a critical value \mathcal{V} we classify an estimate \hat{c} as correct if $m_{\hat{c}} := \min_{c \in C} |\hat{c} - c| \leq \mathcal{V}$. Let $\hat{C}_{\mathcal{V}}$ denote the set of all correct estimates w.r.t. \mathcal{V} . Then \hat{C}_T is the set of all estimates. We compute $|\hat{C}_T|$, and for $\mathcal{V} \in \{10, 5, 2\}$ both $|\hat{C}_{\mathcal{V}}|$ and the mean absolute deviation $M_{\mathcal{V}} := |\hat{C}_{\mathcal{V}}|^{-1} \sum_{\hat{c} \in \hat{C}_{\mathcal{V}}} m_{\hat{c}}$. The results, depending on the scenarios and distributions, are reported in Tables 2–4.

We summarize the results. Scenarios 1a and 1b are well-posed in the sense that results are strong and yield precise estimates: $|\hat{C}_T|$ is close to 5000 over all scenarios and distributions. Notably, in 1a it is exactly $|\hat{C}_{10}| = 5000$ throughout, and $|\hat{C}_5| = 5000$ for three distributions. Also, the strict measure $|\hat{C}_2|$ reveals precise results. In 1b we consider varying σ_u , but the estimates remain similarly precise. The setups 2a and 2b are again well-posed: 2a and 2b are pretty similar to 1a and 1b. In setups 3a and 3b performance is slightly reduced as compared

Scenario	C	μ_u	σ_u
1a	100, 300, 500, 700, 900	1, 4, 1, 8, 1, 4	1, 1, 1, 1, 1, 1
1b	100, 300, 500, 700, 900	1, 4, 1, 8, 1, 4	1, 2, 1, 2, 1, 2
1c	100, 300, 500, 700, 900	0.5, 2, 0.5, 4, 0.5, 2	1, 1, 1, 1, 1, 1
2a	300, 400, 500, 600, 700	1, 4, 1, 8, 1, 4	1, 1, 1, 1, 1, 1
2b	300, 400, 500, 600, 700	1, 4, 1, 8, 1, 4	1, 2, 1, 2, 1, 2
2c	300, 400, 500, 600, 700	0.5, 2, 0.5, 4, 0.5, 2	1, 1, 1, 1, 1, 1
3a	200, 500, 550, 600, 750	1, 4, 1, 8, 1, 4	1, 1, 1, 1, 1, 1
3b	200, 500, 550, 600, 750	1, 4, 1, 8, 1, 4	1, 2, 1, 2, 1, 2
3c	200, 500, 550, 600, 750	0.5, 2, 0.5, 4, 0.5, 2	1, 1, 1, 1, 1, 1
3d	200, 500, 550, 600, 750	0.5, 2, 0.5, 4, 0.5, 2	1, 2, 1, 2, 1, 2
3e	200, 500, 550, 600, 750	1, 2, 4, 8, 4, 2	1, 1, 1, 1, 1, 1

Table 1: Scenarios of C , μ and σ considered in simulations.

Scenario	Distribution	$ \hat{C}_T $	$ \hat{C}_{10} , M_{10}$	$ \hat{C}_5 , M_5$	$ \hat{C}_2 , M_2$
1a	A. (normal)	5005	5000, 0.1	5000, 0.1	4994, 0.1
1a	B. (gamma)	5002	5000, 0.1	5000, 0.1	4993, 0.1
1a	C. (Poisson)	5005	5000, 0.4	4993, 0.3	4905, 0.3
1a	D. (binomial)	5005	5000, 0.2	4998, 0.2	4954, 0.2
1a	E. (mix)	5001	5000, 0.1	5000, 0.1	4993, 0.1
1b	A. (normal)	5001	4998, 0.3	4993, 0.3	4906, 0.2
1b	B. (gamma)	5000	5000, 0.3	4997, 0.3	4909, 0.2
1b	E. (mix)	5004	5000, 0.3	4999, 0.3	4906, 0.2
1c	A. (normal)	4951	4935, 0.5	4912, 0.5	4698, 0.4
1c	B. (gamma)	4953	4932, 0.4	4925, 0.4	4823, 0.3
1c	C. (Poisson)	4640	4626, 0.6	4600, 0.6	4370, 0.5
1c	D. (binomial)	4891	4883, 0.6	4858, 0.5	4642, 0.4
1c	E. (mix)	4936	4929, 0.6	4903, 0.5	4707, 0.4

Table 2: Simulation results for scenarios 1a–c.

Scenario	Distribution	$ \hat{C}_T $	$ \hat{C}_{10} , M_{10}$	$ \hat{C}_5 , M_5$	$ \hat{C}_2 , M_2$
2a	A. (normal)	5002	5000, 0.1	5000, 0.1	4993, 0.1
2a	B. (gamma)	5002	5000, 0.1	5000, 0.1	4988, 0.1
2a	C. (Poisson)	5005	5000, 0.3	4998, 0.3	4908, 0.3
2a	D. (binomial)	5002	5000, 0.2	5000, 0.2	4958, 0.2
2a	E. (mix)	5002	5000, 0.1	5000, 0.1	4989, 0.1
2b	A. (normal)	5002	4998, 0.3	4995, 0.3	4914, 0.2
2b	B. (gamma)	5003	5000, 0.3	4998, 0.3	4928, 0.2
2b	E. (mix)	5008	5000, 0.3	4998, 0.3	4935, 0.2
2c	A. (normal)	4884	4873, 0.5	4855, 0.5	4663, 0.4
2c	B. (gamma)	4906	4870, 0.4	4863, 0.3	4766, 0.3
2c	C. (Poisson)	4553	4541, 0.7	4520, 0.6	4285, 0.5
2c	D. (binomial)	4847	4841, 0.5	4828, 0.5	4647, 0.4
2c	E. (mix)	4926	4920, 0.5	4902, 0.5	4720, 0.4

Table 3: Simulation results for scenarios 2a–c.

Scenario	Distribution	$ \hat{C}_T $	$ \hat{C}_{10} , M_{10}$	$ \hat{C}_5 , M_5$	$ \hat{C}_2 , M_2$
3a	A. (normal)	5004	4990, 0.3	4910, 0.2	4846, 0.1
3a	B. (gamma)	5002	4990, 0.3	4879, 0.2	4828, 0.1
3a	C. (Poisson)	4942	4876, 0.9	4580, 0.5	4334, 0.3
3a	D. (binomial)	5005	4965, 0.6	4787, 0.3	4652, 0.2
3a	E. (mix)	5000	4991, 0.3	4901, 0.1	4857, 0.1
3b	A. (normal)	4988	4928, 0.8	4657, 0.4	4478, 0.3
3b	B. (gamma)	4995	4939, 0.8	4689, 0.4	4482, 0.2
3b	E. (mix)	5001	4947, 0.6	4789, 0.3	4638, 0.2
3c	A. (normal)	4814	4703, 1.3	4286, 0.7	3936, 0.4
3c	B. (gamma)	4820	4749, 1.2	4334, 0.5	4095, 0.3
3c	C. (Poisson)	4387	4249, 1.5	3845, 0.8	3480, 0.5
3c	D. (binomial)	4750	4644, 1.5	4146, 0.7	3809, 0.4
3c	E. (mix)	4856	4756, 1.3	4334, 0.7	3990, 0.4
3d	A. (normal)	3093	2946, 1.6	2620, 0.8	2380, 0.5
3d	B. (gamma)	2962	2842, 1.8	2472, 0.8	2193, 0.4
3d	E. (mix)	2896	2804, 1.4	2548, 0.7	2296, 0.4
3e	A. (normal)	4680	4566, 1.1	4257, 0.5	3984, 0.3
3e	B. (gamma)	4735	4620, 1.0	4302, 0.5	4046, 0.3
3e	C. (Poisson)	3411	3085, 2.3	2584, 1.2	2154, 0.6
3e	D. (binomial)	4129	3883, 1.8	3346, 0.8	2959, 0.4
3e	E. (mix)	4220	4014, 1.8	3452, 0.8	3070, 0.4

Table 4: Simulation results for scenarios 3a-e.

to 2a and 2b due to closer distances. Nevertheless, we obtain about 5000 estimates at precise location for 3a and 3b. In scenarios 1c, 2c and 3c we have jump sizes halved as compared to 1a-3a and 1b-3b. Here, deficiencies start to arise: $|\hat{C}_T|$ reduces to about 4750 to 4950 for distributions A., B., D. and E., while for C., it drops to about 4400 to 4800. In scenario 3d we reduced the effects w.r.t. both smaller jump sizes and higher variances, resulting in higher performance losses as we obtain only around 3000 estimates. But note that e.g., for c_6 it is $\mu_6 - \mu_5 = 1.5$ with $\sigma_6 = 2$ which is reasonably hard to be detected, also taking into account the smaller spacings between c_u . Despite the reduced number, the precision for detected estimates is kept high. Scenario 3e is another example with different jump sizes resulting in a good overall outcome, but slightly weaker than 3a as effects are reduced similarly to 3c. Overall, MSCP yields reliable results over different scenarios of change points and effects: both the number and the locations are reliably estimated. Notably, performance is also kept over different distributions and regardless of changes in variance.

Comparison with state of the art methods We present simulation studies which reveal competitiveness of `mscp` with existing change point detection methods available on CRAN. For all competitors we consider the scenarios 1c, 2c and 3c, see Table 1, and all distributions A.–E. from the previous paragraph. The reason for the choice of these scenarios is that for MSCP deficiencies in detection started to arise. Again, for each such setup we run 1000 simulations which yields 5000 change points in total.

Note that between the three scenarios the locations of C vary while $\mu_u = 0.5, 2, 0.5, 4, 0.5, 2$ and $\sigma_u = 1, \dots, 1$ remain unchanged. In particular, due to constant σ_u , results should not be

affected through a method’s capability of handling changes in variance, which holds true for MSCP. For that also keep in mind that, in fact, $\sigma_u \equiv 1$ only holds true for A. B. and parts of E., while for C. and D. σ_u always changes with μ_u .

As competitors of `mscp` we consider `mosum` Meier et al. (2021) with individual windows $G=50, 100$ and 200 , respectively, `wbs` Baranowski and Fryzlewicz (2019), `not` Baranowski et al. (2019b) with `contrast=pcwsConstMeanVar` and `pcwsConstMeanHT`, respectively, `changePoint` Killick et al. (2016) considering `cpt.meanvar` with `method=PELT` and `test.stat='Normal'` for A. D. and E., `'Gamma'` for B., and `'Poisson'` for C., `stepR` Pein et al. (2020) with `stepFit`, `cumSeg` Muggeo (2020) using `jumpoints`, and `FDRSeg` Li and Sieling (2017) using `fdrseg` with `sd` estimating the global standard deviation. Any other tuning-parameters are kept default.

The results are presented in Table 5 (scenario 1c), Table 6 (scn. 2c) and Table 7 (scn. 3c). We first recall that overall, `mscp` yields a total number of estimates $|\hat{C}_T|$ of about 4750 to 4950 for distributions A., B., D. and E., and about 4400 to 4800 for C. Further, recall high estimation precision regarding different levels of tolerance, i.e., values of $|\hat{C}_V|$ and M_V for $V = \{10, 5, 2\}$. In total, also the competitors often show a similar performance in many scenarios, but also somewhat weaken in certain setups. For `mosum` we nicely see, e.g., in Table 5 A., that performance depends on the selection of the individual window. For example we find $G=50$ to slightly overestimate, and $G=200$ to underestimate the total number of change points, while the middle window $G=100$ performs best, also noting slightly reduced location precision for small windows as compared to `mscp`. Note that overall the problem of a fixed window becomes even more evident when change point distances are reduced, see Table 6 and 7, particularly because large windows lose sensitivity. Of course, window selection is a major challenge in practice as change point locations are unknown, and `mscp` circumvents it by nature. Apart from this, `mosum` yields quite stable results among different distributions, but similar to `mscp` it loses power for distribution C. For `wbs` we find good performance for distribution A., w.r.t. both the number and precision of estimates over all scenarios, while it tends to overestimate for other distributions, most extreme for C. and B. We overall find good performance for the method `not`. However, we mention that `contrast=pcwsConstMeanVar` tends to overestimate particularly for distribution B., noting that the contrast assumes normality. Interestingly, `contrast=pcwsConstMeanHT`, which assumes heavy-tailed additive errors, overall performs nicely, while showing somewhat reduced estimation precision, as compared to `mscp`. For `changePoint` we find great performance for A. and C. where parametric assumptions are met, but tremendous overestimation if not, see D. and E. Although parametric assumptions are met in B., it also overestimates. `stepR` shows reliable results in A., while it tends to overestimate the number of change points if normality is violated. This tendency is less drastic in E. where the distribution is normal in at least two sections, or D., but more problematic for distribution B. Over all setups `cumSeg` perform nicely and only very slightly overestimates the number of change points, but shows somewhat reduced estimation precision as compared to `mscp`. `FDRSeg` also shows good performance among almost all setups presented, w.r.t. both different scenarios and distributions. However, we mention overestimation in C., and a slight reduction in estimation precision as compared to `mscp`.

In summary, the results presented reveal serious competitiveness of `mscp` with state of the art change point detection methods. Particularly, `mscp` overcomes the selection of a tuning bandwidth as compared to single window MOSUM techniques. Also, the consideration of sce-

narios 1c–3c reveals comparably good performance regarding different change point distances. Besides that, a comparably stable performance over different distributions supports the value of the non-parametric nature of `mscp` for practice.

Scn.	Distr.	Method	$ \hat{C}_T $	$ \hat{C}_{10} , M_{10}$	$ \hat{C}_5 , M_5$	$ \hat{C}_2 , M_2$
1c	A. (normal)	<code>mscp</code>	4951	4935, 0.5	4912, 0.5	4698, 0.4
		<code>mosum</code> $G = 50$	5057	4965, 0.9	4809, 0.7	4378, 0.4
		<code>mosum</code> $G = 100$	5002	4969, 0.8	4852, 0.7	4430, 0.4
		<code>mosum</code> $G = 200$	4002	3972, 0.4	3905, 0.3	3757, 0.2
		<code>wbs</code>	5030	4983, 0.7	4890, 0.6	4529, 0.4
		not 'MeanVar'	5007	4986, 0.7	4886, 0.6	4517, 0.4
		not 'MeanHT'	5010	4974, 0.8	4846, 0.6	4438, 0.4
		<code>changepoint</code>	5033	5002, 0.8	4893, 0.6	4523, 0.4
		<code>stepR</code>	5037	4978, 1.4	4863, 1.2	4443, 1
		<code>cumSeg</code>	5019	4935, 1.5	4782, 1.4	3953, 0.9
	<code>FDRSeg</code>	5000	4979, 1.4	4867, 1.2	4446, 1	
	B. (gamma)	<code>mscp</code>	4953	4932, 0.4	4925, 0.4	4823, 0.3
		<code>mosum</code> $G = 50$	5082	4873, 1	4658, 0.7	4223, 0.4
		<code>mosum</code> $G = 100$	5014	4889, 0.9	4696, 0.6	4286, 0.4
		<code>mosum</code> $G = 200$	4005	3948, 0.4	3881, 0.3	3748, 0.2
		<code>wbs</code>	29906	6827, 2.1	5692, 0.9	4846, 0.4
		not 'MeanVar'	15799	5076, 1.9	4342, 0.8	3738, 0.3
		not 'MeanHT'	5029	4991, 0.6	4928, 0.5	4671, 0.3
		<code>changepoint</code>	14342	5529, 2.6	4397, 1.3	3390, 0.5
		<code>stepR</code>	30957	6568, 2.7	5408, 1.5	4504, 1.1
		<code>cumSeg</code>	5033	4911, 1.5	4734, 1.3	4015, 0.9
	<code>FDRSeg</code>	6230	4922, 1.5	4760, 1.3	4330, 1	
	C. (Poisson)	<code>mscp</code>	4640	4626, 0.6	4600, 0.6	4370, 0.5
		<code>mosum</code> $G = 50$	4812	4679, 1.1	4512, 0.9	4002, 0.5
		<code>mosum</code> $G = 100$	4847	4752, 1.1	4561, 0.8	4048, 0.5
		<code>mosum</code> $G = 200$	3900	3886, 0.5	3844, 0.4	3672, 0.2
		<code>wbs</code>	13155	5447, 1.6	4948, 0.9	4276, 0.5
		not 'MeanVar'	5231	4941, 1	4755, 0.8	4276, 0.4
		not 'MeanHT'	5090	4906, 1.1	4679, 0.8	4182, 0.5
		<code>changepoint</code>	5000	4964, 0.9	4834, 0.8	4362, 0.4
		<code>stepR</code>	12518	5253, 2.1	4743, 1.5	3953, 1.1
		<code>cumSeg</code>	5021	4896, 1.8	4637, 1.5	3700, 1
	<code>FDRSeg</code>	5253	4921, 1.7	4685, 1.4	4030, 1.1	
	D. (binomial)	<code>mscp</code>	4891	4883, 0.6	4858, 0.5	4642, 0.4
		<code>mosum</code> $G = 50$	4837	4739, 0.9	4585, 0.7	4165, 0.4
		<code>mosum</code> $G = 100$	4846	4791, 1	4622, 0.7	4189, 0.4
		<code>mosum</code> $G = 200$	3911	3896, 0.4	3854, 0.3	3715, 0.2
		<code>wbs</code>	6472	5035, 1	4816, 0.7	4415, 0.4
		not 'MeanVar'	5184	4972, 0.9	4798, 0.7	4399, 0.4
		not 'MeanHT'	5055	4952, 1	4764, 0.7	4334, 0.4
		<code>changepoint</code>	191707	21855, 4.9	12235, 2.5	6215, 1
		<code>stepR</code>	6369	4987, 1.6	4756, 1.4	4208, 1.1
		<code>cumSeg</code>	5009	4928, 1.6	4726, 1.4	3893, 0.9
	<code>FDRSeg</code>	5001	4953, 1.6	4772, 1.3	4253, 1.1	
	E. (mix)	<code>mscp</code>	4936	4929, 0.6	4903, 0.5	4707, 0.4
		<code>mosum</code> $G = 50$	5040	4971, 0.9	4848, 0.7	4414, 0.4
		<code>mosum</code> $G = 100$	4996	4969, 0.8	4861, 0.7	4472, 0.4
		<code>mosum</code> $G = 200$	4001	3973, 0.4	3912, 0.3	3750, 0.2
		<code>wbs</code>	6406	5056, 0.8	4926, 0.6	4547, 0.4
		not 'MeanVar'	5180	4995, 0.8	4876, 0.6	4504, 0.4
		not 'MeanHT'	5050	4987, 0.8	4894, 0.6	4519, 0.4
		<code>changepoint</code>	76448	11544, 3.9	7751, 1.9	5030, 0.8
		<code>stepR</code>	6288	5020, 1.4	4905, 1.2	4481, 1
		<code>cumSeg</code>	5007	4938, 1.5	4819, 1.3	4034, 0.9
	<code>FDRSeg</code>	5008	4984, 1.3	4909, 1.2	4499, 1	

Table 5: Comparative simulation study w.r.t. scenario 1c.

Data example The complete sequence of a human genome (T2T-CHM13) was recently presented for the first time in Nurk et al. (2022). We analyze the nucleotide sequence of

Scn.	Distr.	Method	$ \hat{C}_T $	$ \hat{C}_{10} , M_{10}$	$ \hat{C}_5 , M_5$	$ \hat{C}_2 , M_2$		
2c	A. (normal)	mscp	4884	4873, 0.5	4855, 0.5	4663, 0.4		
		mosum $G = 50$	5067	4964, 0.9	4798, 0.7	4348, 0.4		
		mosum $G = 100$	5015	4992, 0.4	4935, 0.3	4749, 0.2		
		mosum $G = 200$	3899	1505, 2.3	1266, 1.3	994, 0.6		
		wbs	5021	4985, 0.7	4872, 0.6	4539, 0.4		
		not 'MeanVar'	5019	4991, 0.7	4869, 0.6	4532, 0.4		
		not 'MeanHT'	5008	4977, 0.8	4849, 0.6	4484, 0.4		
		changepoint	5022	4996, 0.8	4887, 0.6	4518, 0.4		
		stepR	5046	4979, 1.4	4859, 1.2	4420, 1		
		cumSeg	5063	4890, 1.7	4633, 1.4	3750, 0.9		
		FDRSeg	5000	4979, 1.4	4860, 1.2	4422, 1		
			B. (gamma)	mscp	4906	4870, 0.4	4863, 0.3	4766, 0.3
				mosum $G = 50$	5073	4881, 1	4659, 0.6	4232, 0.3
mosum $G = 100$	5048			4938, 0.5	4850, 0.3	4646, 0.2		
mosum $G = 200$	3873			1475, 1.9	1269, 1	1060, 0.4		
wbs	30508			6790, 2.1	5658, 0.9	4859, 0.4		
not 'MeanVar'	15290			4989, 2	4217, 0.9	3614, 0.3		
not 'MeanHT'	5041			4985, 0.6	4917, 0.5	4662, 0.3		
changepoint	14300			5495, 2.5	4407, 1.2	3420, 0.4		
stepR	32218			6701, 2.7	5464, 1.5	4518, 1		
cumSeg	5063			4850, 1.7	4603, 1.4	3792, 0.9		
FDRSeg	7008			4965, 1.5	4763, 1.3	4331, 1		
	C. (Poisson)			mscp	4553	4541, 0.7	4520, 0.6	4285, 0.5
				mosum $G = 50$	4820	4682, 1.1	4482, 0.8	3984, 0.5
		mosum $G = 100$	4741	4681, 0.5	4609, 0.4	4396, 0.2		
		mosum $G = 200$	3394	1354, 1.9	1193, 1.2	976, 0.6		
		wbs	10456	5351, 1.5	4907, 0.9	4270, 0.5		
		not 'MeanVar'	5215	4930, 1.1	4729, 0.8	4228, 0.5		
		not 'MeanHT'	5094	4893, 1.2	4662, 0.8	4136, 0.5		
		changepoint	5000	4966, 0.9	4818, 0.7	4361, 0.4		
		stepR	9851	5223, 2.1	4718, 1.5	3916, 1.1		
		cumSeg	5039	4791, 1.9	4487, 1.6	3488, 1		
		FDRSeg	5742	4998, 1.8	4689, 1.4	3992, 1.1		
			D. (binomial)	mscp	4847	4841, 0.5	4828, 0.5	4647, 0.4
				mosum $G = 50$	4835	4728, 0.9	4600, 0.7	4173, 0.4
mosum $G = 100$	4799			4757, 0.4	4711, 0.3	4538, 0.2		
mosum $G = 200$	3415			1389, 1.8	1247, 1.1	1049, 0.6		
wbs	5984			5004, 0.9	4837, 0.7	4430, 0.4		
not 'MeanVar'	5168			4957, 0.9	4807, 0.7	4426, 0.4		
not 'MeanHT'	5076			4949, 1	4775, 0.7	4349, 0.4		
changepoint	195010			21834, 4.9	12190, 2.5	6114, 1		
stepR	5904			4988, 1.6	4786, 1.3	4219, 1		
cumSeg	5030			4864, 1.7	4615, 1.4	3748, 0.9		
FDRSeg	5034			4953, 1.5	4803, 1.3	4245, 1		
	E. (mix)			mscp	4926	4920, 0.5	4902, 0.5	4720, 0.4
				mosum $G = 50$	5042	4963, 0.8	4859, 0.7	4469, 0.4
		mosum $G = 100$	5026	4991, 0.4	4950, 0.3	4794, 0.2		
		mosum $G = 200$	3822	1551, 2	1357, 1.2	1110, 0.6		
		wbs	5880	5058, 0.8	4954, 0.6	4600, 0.4		
		not 'MeanVar'	5113	4990, 0.7	4898, 0.6	4542, 0.4		
		not 'MeanHT'	5022	4981, 0.8	4883, 0.7	4514, 0.4		
		changepoint	40166	11549, 3.9	7748, 1.9	5000, 0.8		
		stepR	5863	5042, 1.4	4920, 1.2	4484, 1		
		cumSeg	5053	4895, 1.7	4682, 1.4	3835, 0.9		
		FDRSeg	5044	4996, 1.3	4917, 1.2	4510, 1		

Table 6: Comparative simulation study w.r.t. scenario 2c.

the X-chromosome (Homo sapiens isolate CHM13 chromosome X, GenBank: CP068255.2). It consists of about $b = 1542 \cdot 10^5$ base pairs. We segment the sequence into segments of length $d = 2 \cdot 10^5$, within which we compute the frequency of the base cytosine. This yields $T = b/d = 771$ data points to which we apply MSCP, see Figure 10.

Nine change points were estimated, $\hat{C} = \{20, 80, 124, 181, 383, 479, 635, 699, 739\}$, yielding parameter estimates $\hat{\mu}_u \approx (45, 40, 41, 37, 41, 36, 39, 40, 38, 44) \cdot 10^3$ and

Scn.	Distr.	Method	$ \hat{C}_T $	$ \hat{C}_{10} , M_{10}$	$ \hat{C}_5 , M_5$	$ \hat{C}_2 , M_2$		
3c	A. (normal)	mscp	4814	4703, 1.3	4286, 0.7	3936, 0.4		
		mosum $G = 50$	5063	4955, 0.8	4823, 0.6	4452, 0.3		
		mosum $G = 100$	4344	2665, 1.7	2445, 1.2	2008, 0.6		
		mosum $G = 200$	3055	2032, 0.8	1983, 0.6	1823, 0.4		
		wbs	5018	4975, 0.7	4873, 0.6	4519, 0.4		
		not 'MeanVar'	5009	4980, 0.8	4866, 0.6	4510, 0.4		
		not 'MeanHT'	5012	4973, 0.8	4832, 0.6	4423, 0.4		
		changepoint	5026	5003, 0.8	4894, 0.6	4532, 0.4		
		stepR	5045	4973, 1.4	4855, 1.2	4445, 1		
		cumSeg	5086	4831, 1.7	4587, 1.4	3824, 0.9		
		FDRSeg	5000	4976, 1.4	4860, 1.2	4449, 1		
			B. (gamma)	mscp	4820	4749, 1.2	4334, 0.5	4095, 0.3
				mosum $G = 50$	5096	4903, 0.8	4719, 0.6	4360, 0.3
				mosum $G = 100$	4377	2572, 1.7	2310, 1	1938, 0.5
mosum $G = 200$	3076			2023, 0.9	1942, 0.6	1780, 0.3		
wbs	23085			6251, 1.7	5425, 0.8	4767, 0.4		
not 'MeanVar'	13558			5090, 1.9	4344, 0.9	3744, 0.4		
not 'MeanHT'	5021			4988, 0.6	4927, 0.5	4667, 0.3		
changepoint	12527			5541, 2.6	4437, 1.3	3411, 0.4		
stepR	23771			6141, 2.4	5188, 1.4	4451, 1		
cumSeg	5085			4812, 1.6	4598, 1.3	3859, 0.8		
FDRSeg	7424			5046, 1.7	4746, 1.3	4327, 1		
	C. (Poisson)			mscp	4387	4249, 1.5	3845, 0.8	3480, 0.5
				mosum $G = 50$	4860	4703, 0.9	4531, 0.6	4133, 0.3
				mosum $G = 100$	3605	2295, 1.8	2075, 1.2	1693, 0.6
		mosum $G = 200$	3021	1989, 1	1904, 0.8	1731, 0.5		
		wbs	9732	5336, 1.5	4889, 0.9	4223, 0.5		
		not 'MeanVar'	5226	4910, 1.1	4683, 0.8	4184, 0.5		
		not 'MeanHT'	5039	4901, 1.2	4670, 0.9	4122, 0.5		
		changepoint	5002	4975, 0.9	4846, 0.7	4408, 0.4		
		stepR	9140	5176, 2.1	4660, 1.5	3894, 1.1		
		cumSeg	5027	4559, 1.7	4346, 1.5	3561, 1		
		FDRSeg	5928	5156, 2	4724, 1.5	3986, 1.1		
			D. (binomial)	mscp	4750	4644, 1.5	4146, 0.7	3809, 0.4
				mosum $G = 50$	4870	4786, 0.8	4655, 0.6	4284, 0.3
				mosum $G = 100$	3703	2347, 1.6	2160, 1.1	1819, 0.6
mosum $G = 200$	2974			1970, 0.8	1935, 0.6	1796, 0.4		
wbs	5920			5006, 0.9	4837, 0.7	4409, 0.4		
not 'MeanVar'	5113			4962, 0.9	4819, 0.7	4405, 0.4		
not 'MeanHT'	5052			4955, 1	4778, 0.7	4337, 0.4		
changepoint	185641			21685, 4.9	12126, 2.5	6151, 1		
stepR	5851			4962, 1.6	4761, 1.4	4206, 1		
cumSeg	5093			4690, 1.6	4515, 1.4	3756, 0.9		
FDRSeg	5093			4967, 1.5	4792, 1.3	4262, 1		
	E. (mix)			mscp	4856	4756, 1.3	4334, 0.7	3990, 0.4
				mosum $G = 50$	5060	4983, 0.7	4866, 0.6	4538, 0.3
				mosum $G = 100$	4339	2650, 1.6	2446, 1.1	2052, 0.6
		mosum $G = 200$	3059	2045, 0.8	1992, 0.7	1841, 0.4		
		wbs	6026	5082, 0.8	4957, 0.7	4581, 0.4		
		not 'MeanVar'	5094	4991, 0.8	4895, 0.6	4547, 0.4		
		not 'MeanHT'	5012	4982, 0.8	4883, 0.6	4524, 0.4		
		changepoint	21991	11491, 3.8	7769, 1.9	5059, 0.8		
		stepR	5938	5052, 1.4	4914, 1.3	4461, 1		
		cumSeg	5069	4818, 1.6	4620, 1.4	3833, 0.9		
		FDRSeg	5174	5030, 1.4	4915, 1.2	4485, 1		

Table 7: Comparative simulation study w.r.t. scenario 3c.

$\hat{\sigma}_u \approx (4.5, 2.3, 2.5, 1.5, 3.2, 1.0, 2.6, 2.1, 1.5, 5.7) \cdot 10^3$. The segmentation closely aligns with visual inspection. We note that model assumptions are fairly met: first, an increase in mean is accompanied with an increase in variance, and vice versa, which aligns with the assumption that the theoretical variance may also change when change in expectation occurs. Second, in each section, serial correlation proves to be moderate (e.g., for lag one it is between 0.3 (section 6) and 0.7 (last section 10), and it rapidly decreases for higher lags). Third, the

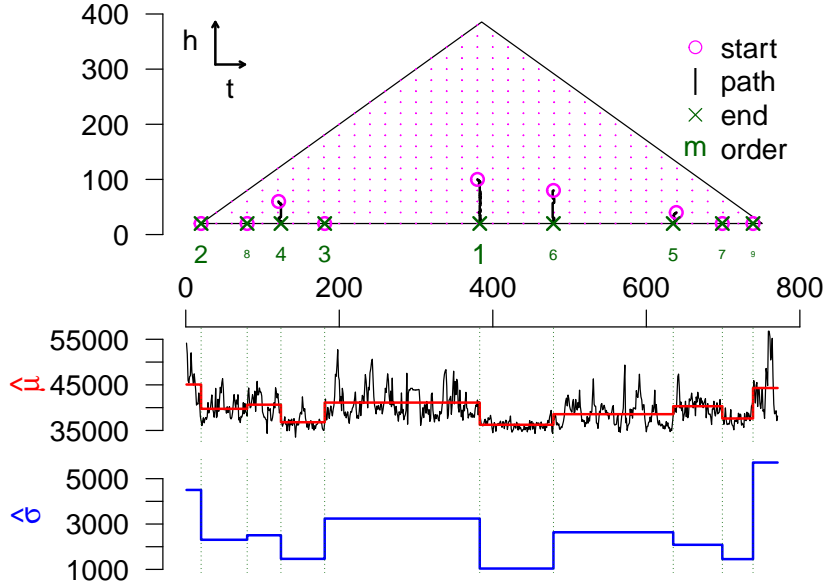


Figure 10: Analysis of the base cytosine in the X-chromosome of T2T-CHM13.

representation of the data as frequency counts is supported by the non-parametric assumptions on the distributions. Finally, we mention that the result is stable under variation of d . Being an interesting result in itself, the example shows that MSCP can be helpful for the segmentation of genomic data: yielding segments with relatively stable first order moments, it can be considered a preprocessing step in data analysis.

6 Appendix

Proof of Lemma 3.1: W.l.o.g. let $j = \ell$. For $\hat{\mu}_\ell^{(k)}$ first let $C = \emptyset$ where we need to show $n^v \cdot (\hat{\mu}_\ell^{(k)} - \mu^{(k)})_{(t,h)} \rightarrow (0)_{(t,h)}$ a.s. as $n \rightarrow \infty$. We show some uniform convergence w.r.t $[0, T]$ and then extend considerations to Δ_δ . It holds a.s. as $n \rightarrow \infty$

$$n^v \cdot \sup_{t \in [0, T]} \left| \frac{1}{n} \sum_{i=1}^{\lfloor nt \rfloor} X_i^k - t\mu^{(k)} \right| \rightarrow 0, \quad (13)$$

$$\text{for } v \in \begin{cases} (-\infty, 1/2), & \text{if } k = 1, \\ (-\infty, 1/2) \cap (-\infty, p/(p+2)], & \text{if } k = 2. \end{cases}$$

For this, first apply Marcinkiewicz-Zygmund (MZ)-SLLN to $(X_i)_i$ and $(X_i^2)_i$: For $(X_i)_i$ note that for any $\alpha \in (0, 2)$ it is $\mathbb{E}[|X_i|^\alpha] < \infty$, and thus for $k = 1$ a.s. as $n \rightarrow \infty$

$$n^{(\alpha-1)/\alpha} \cdot \left(\frac{1}{n} \sum_{i=1}^n X_i^k - \mu^{(k)} \right) = n^{-1/\alpha} \cdot \left(\sum_{i=1}^n X_i^k - n\mu^{(k)} \right) \rightarrow 0. \quad (14)$$

For the squares $(X_i^2)_i$ we choose $\alpha \in (0, (2+p)/2]$ if $p < 2$ and $\alpha \in (0, 2)$ if $p \geq 2$. Then $\mathbb{E}[|X_i^2|^\alpha] < \infty$ and thus (14) applies for $k = 2$. As $(\alpha - 1)/\alpha \leq p/(2+p)$ if $p < 2$, and

$(\alpha - 1)/\alpha < 1/2$ if $p \geq 2$, we obtain for $k = 1, 2$ a.s. as $n \rightarrow \infty$

$$n^v \cdot \left(\frac{1}{n} \sum_{i=1}^n X_i^k - \mu^{(k)} \right) \rightarrow 0, \text{ for } v \in \begin{cases} (-\infty, 1/2), & \text{if } k = 1, \\ (-\infty, 1/2) \cap (-\infty, p/(p+2)], & \text{if } k = 2. \end{cases} \quad (15)$$

For uniform convergence in (13) we discretize time and apply (15), a.s. as $n \rightarrow \infty$

$$\begin{aligned} n^v \cdot \sup_{0 \leq t \leq T} \left| \frac{1}{n} \sum_{i=1}^{\lfloor nt \rfloor} X_i^k - t \mu^{(k)} \right| &\leq n^v \cdot \sup_{0 \leq t \leq T} \left| \frac{1}{n} \sum_{i=1}^{\lfloor nt \rfloor} X_i^k - \frac{\lfloor nt \rfloor}{n} \mu^{(k)} \right| + r_n \\ &= n^v \cdot \max_{m \in \{1, 2, \dots, nT\}} \left| \frac{1}{n} \sum_{i=1}^m X_i^k - \frac{m}{n} \mu^{(k)} \right| + r_n \rightarrow 0, \end{aligned}$$

as $r_n := n^v \cdot \sup_{t \in [0, T]} |t - \lfloor nt \rfloor / n| \mu^{(k)} \leq n^v \cdot (1/n) \mu^{(k)} \rightarrow 0$ as $n \rightarrow \infty$, and for $\varepsilon > 0$

$$\begin{aligned} n^v \cdot \max_{m \in \{1, 2, \dots, nT\}} \left| \frac{1}{n} \sum_{i=1}^m X_i^k - \frac{m}{n} \mu^{(k)} \right| &\leq \\ n^v \cdot \frac{1}{n} \max_{m \leq m_0} \left| \sum_{i=1}^m X_i^k - m \mu^{(k)} \right| &+ T^{1-v} \max_{m_0 < m \leq nT} \left(\frac{m}{nT} \right)^{1-v} m^v \cdot \left| \frac{1}{m} \sum_{i=1}^m X_i^k - \mu^{(k)} \right| \leq \varepsilon \end{aligned}$$

a.s. for n large enough, as the maximum in the first summand is independent from n , and for the second summand note $(m/nT)^{1-v} \leq 1$ and (15) yields that for almost every realization we find $m_0 \in \mathbb{N}$ such that $m^v \cdot |(1/m) \sum_{i=1}^m X_i^k - \mu^{(k)}| < T^{v-1} \varepsilon / 2$ for all $m > m_0$. Thus, (13) holds. Now we consider Δ_δ . As $0 \leq t - h \leq T$ for all $(t, h) \in \Delta_\delta$, (13) yields a.s. as $n \rightarrow \infty$

$$\begin{aligned} n^v \cdot \sup_{(t, h) \in \Delta_\delta} \left| \frac{1}{n} \sum_{i=1}^{\lfloor nt \rfloor} X_i^k - t \mu^{(k)} \right| &\rightarrow 0 \quad \text{and} \\ n^v \cdot \sup_{(t, h) \in \Delta_\delta} \left| \frac{1}{n} \sum_{i=1}^{\lfloor n(t-h) \rfloor} X_i^k - (t-h) \mu^{(k)} \right| &\rightarrow 0, \end{aligned}$$

We include the factor $1/h \geq 2/T > 0$ and obtain in $(\mathcal{D}_{\mathbb{R}}[\Delta_\delta], \|\cdot\|_\infty)$ a.s. as $n \rightarrow \infty$

$$\begin{aligned} n^v \cdot (\hat{\mu}_\ell^{(k)} - \mu^{(k)})_{(t, h)} &= \\ n^v \cdot \left[\left(\frac{1}{nh} \sum_{i=1}^{\lfloor nt \rfloor} X_i^k - \frac{t}{h} \mu^{(k)} \right) - \left(\frac{1}{nh} \sum_{i=1}^{\lfloor n(t-h) \rfloor} X_i^k - \frac{t-h}{h} \mu^{(k)} \right) \right]_{(t, h)} &\rightarrow (0)_{(t, h)}. \end{aligned} \quad (16)$$

Now let $C \neq \emptyset$. We segment $(t-h, t]$ according to C and find $\hat{\mu}_\ell^{(k)} - \mu^{(k)}$ as

$$\sum_{u=1}^{|C_\ell|+1} \left(\left[\frac{\lfloor nc_{\ell, u} \rfloor - \lfloor nc_{\ell, u-1} \rfloor}{nh} \cdot \frac{1}{\lfloor nc_{\ell, u} \rfloor - \lfloor nc_{\ell, u-1} \rfloor} \sum_{i=\lfloor nc_{\ell, u-1} \rfloor + 1}^{\lfloor nc_{\ell, u} \rfloor} X_i^k \right] - \frac{d_{\ell, u}}{h} \cdot \mu_{\ell, u}^{(k)} \right). \quad (17)$$

The u -th summand refers to a subsection that relates to the error sequence $(Z_{u, i})_{i=1, 2, \dots}$ and

in which X_i equals $\mu_u + \sigma_u \cdot Z_{u,i}$. From (16) we conclude a.s. as $n \rightarrow \infty$

$$n^v \cdot \sup_{1 \leq d \leq t \leq T} \left| \frac{1}{[nd]} \sum_{i=[n(t-d)+1}^{[nt]} (\mu_u + \sigma_u \cdot Z_{u,i})^k - \mu_u^{(k)} \right| \rightarrow 0, \quad (18)$$

which states uniform convergence w.r.t all subintervals of varying length d . When including the factor $d/h \geq 1$ and summing over all u , the expression still vanishes a.s. as $n \rightarrow \infty$, and it states an upper bound for $n^v \cdot \sup_{(t,h) \in \Delta_\delta} |\hat{\mu}_\ell^{(k)} - \tilde{\mu}_\ell^{(k)}|$.

Regarding $\hat{\sigma}_\ell^2$ we decompose in the u -th subsection $(X_i - \hat{\mu}_\ell)^2 = (X_i - \mu_{\ell,u})^2 - 2(X_i - \mu_{\ell,u})(\hat{\mu}_\ell - \mu_{\ell,u}) + (\hat{\mu}_\ell - \mu_{\ell,u})^2$. Averages in the subsection tend to $\sigma_{\ell,u}^2 + 0 + (\tilde{\mu}_\ell - \mu_{\ell,u})^2$, and summation over subsections yields a.s. as $n \rightarrow \infty$ that $n^v \cdot \sup_{(t,h) \in \Delta_\delta} |\hat{\sigma}_\ell^2 - \tilde{\sigma}_\ell^2| \rightarrow 0$, as before using MZ-SLLN and discretization arguments. \square

Proof of Lemma 3.3: Continuity is inherited from the limits in (5) and (6). W.l.o.g. consider $c_1 =: c$. As $v_{t,h} \geq 1$ with equality at c it is $v_{t,h} \cdot |d_{t,h}^{(n)}| \geq |d_{t,h}^{(n)}|$. $\tilde{\mu}_r - \tilde{\mu}_\ell$ has the shape of a hat: it is zero outside the h -neighborhood of c , it is $\mu_2 - \mu_1$ at c , and it is linearly interpolated in between. $\tilde{\sigma}_r^2 + \tilde{\sigma}_\ell^2$ is $2\sigma_1^2$ left of $c - h$, and $2\sigma_2^2$ right of $c + h$, and linearly interpolated in between. Thus, in the h -neighborhood of c the root $(\tilde{\sigma}_r^2 + \tilde{\sigma}_\ell^2)^{1/2}$ is constant if $\sigma_2^2 = \sigma_1^2$, it is strictly convex if $\sigma_2^2 > \sigma_1^2$ and strictly concave if $\sigma_2^2 < \sigma_1^2$. As the numerator is piecewise linear, i.e., of order t , and the denominator of order $t^{1/2}$, the statements about the curvatures of $v_{t,h} \cdot d_{t,h}^{(n)}$ hold true. We now turn to $d_{t,h}^{(n)}$. We represent $\tilde{\sigma}_j^2$ through $\tilde{\sigma}_j^2$ plus errors

$$\tilde{\sigma}_j^2 = \sum_{u=1}^2 \frac{d_u}{h} \cdot [\sigma_u^2 + (\tilde{\mu}_j - \mu_u)^2] = \tilde{\sigma}_j^2 + \frac{d_1 d_2}{h^2} \cdot (\mu_2 - \mu_1)^2,$$

for $j \in \{\ell, r\}$, i.e., we find the error as $e_j^2 := [d_1 d_2 / h^2] (\mu_2 - \mu_1)^2$. We abbreviated $d_u := d_{j,u}$. Note that $e_\ell^2 = e_r^2$, and set $x := d_1/h$ and $d_2/h = (1-h)/h = (1-x)$ with $x \in [0, 1]$, which yields a representation through the proportions of the window left and right of c . Note that the error $e_j^2 = x(1-x) \cdot (\mu_2 - \mu_1)^2$ is quadratic and maximal for $x = 1/2$, thus taking the value $(\mu_2 - \mu_1)^2/4$, which is plausible as half of the window refers to the left and the other half to the right population. Within both $[c-h, c]$ and $(c, c+h]$ it holds that $\tilde{\mu}_r - \tilde{\mu}_\ell$ is linear in x and the denominator of $d_{t,h}^{(n)}$ is now the root of first function $\tilde{\sigma}_r^2 + \tilde{\sigma}_\ell^2$ which is linear in x plus second the quadratic error e_j^2 . W.l.o.g. we consider $t \in [c-h, c]$ where the right window contains c . Then we find $d_{t,h}^{(n)}$ as a function f of x as

$$f(x) = \sqrt{nh} \cdot \frac{(\mu_2 - \mu_1) \cdot x}{\sqrt{[(\sigma_2^2 - \sigma_1^2) \cdot x + 2\sigma_1^2] + [(\mu_2 - \mu_1)^2 \cdot x \cdot (1-x)]}}, \quad x \in [0, 1],$$

for all valid $h \in (\delta, T/2]$, which yields the derivative w.r.t. x

$$f'(x) = \sqrt{nh} \cdot (\mu_2 - \mu_1) \cdot \frac{2^{-1}[(\sigma_2^2 - \sigma_1^2) + (\mu_2 - \mu_1)^2] \cdot x + 2\sigma_1^2}{[(\sigma_2^2 - \sigma_1^2) \cdot x + 2\sigma_1^2 + (\mu_2 - \mu_1)^2 \cdot x \cdot (1-x)]^{3/2}}.$$

In (19) we see that the fraction is positive and thus $f'(x) > 0$ if $\mu_2 > \mu_1$ and $f'(x) < 0$ if $\mu_2 < \mu_1$, which gives (8). To bound $|f'(x)|$ we find the numerator $\geq 2^{-1}[\sigma_2^2 + 3\sigma_1^2 + (\mu_2 - \mu_1)^2] \wedge 2\sigma_1^2$

and for the denominator we get $(\sigma_2^2 - \sigma_1^2)x + 2\sigma_1^2 \leq 2(\sigma_2^2 \vee \sigma_1^2)$ and $x(1-x) \leq 1/4$, such that

$$\begin{aligned} |f'(x)| &\geq \sqrt{nh} \cdot |\mu_2 - \mu_1| \cdot \frac{2^{-1}[\sigma_2^2 + 3\sigma_1^2 + (\mu_2 - \mu_1)^2] \wedge 2\sigma_1^2}{[2(\sigma_2^2 \vee \sigma_1^2) + (\mu_2 - \mu_1)^2/4]^{3/2}} \\ &\geq \sqrt{nh} \cdot |\mu_2 - \mu_1| \cdot \frac{2(\sigma_2^2 \wedge \sigma_1^2)}{[2(\sigma_2^2 \vee \sigma_1^2) + (\mu_2 - \mu_1)^2/4]^{3/2}} > 0. \end{aligned} \quad (19)$$

In the second inequality we omitted $(\mu_2 - \mu_1)^2 \geq 0$ and used that $2\sigma_1^2 < 2^{-1}[\sigma_2^2 + 3\sigma_1^2]$ iff $\sigma_1^2 < \sigma_2^2$. This is the lower bound in (9). For the upper bound we find the numerator $\leq 2^{-1}[\sigma_2^2 + 3\sigma_1^2 + (\mu_2 - \mu_1)^2] \vee 2\sigma_1^2 \leq 2(\sigma_2^2 \vee \sigma_1^2) + (\mu_2 - \mu_1)^2$, and for the denominator we mention $(\sigma_2^2 - \sigma_1^2)x + 2\sigma_1^2 \geq 2(\sigma_2^2 \wedge \sigma_1^2)$ such that

$$|f'(x)| \leq \sqrt{nh} \cdot |\mu_2 - \mu_1| \cdot \frac{2(\sigma_2^2 \vee \sigma_1^2) + (\mu_2 - \mu_1)^2}{[2(\sigma_2^2 \wedge \sigma_1^2)]^{3/2}},$$

which completes (9). \square

Proof of Proposition 3.4: Donsker's theorem yields in $(\mathcal{D}_{\mathbb{R}}[0, T], \|\cdot\|_{\infty})$ as $n \rightarrow \infty$

$$\left[\frac{1}{\sigma\sqrt{n}} \cdot \sum_{i=1}^{\lfloor nt \rfloor} (X_i - \mu) \right]_t \xrightarrow{d} (W_t)_t. \quad (20)$$

Define a continuous map φ from $(\mathcal{D}_{\mathbb{R}}[0, T], \|\cdot\|_{\infty})$ to $(\mathcal{D}_{\mathbb{R}}[\Delta_{\delta}], \|\cdot\|_{\infty})$ via

$$\varphi : (f(t))_t \rightarrow \left(\frac{[f(t+h) - f(t)] - [f(t) - f(t-h)]}{\sqrt{2h}} \right)_t,$$

and apply φ on (20). The continuous mapping yields in $(\mathcal{D}_{\mathbb{R}}[\Delta_{\delta}], \|\cdot\|_{\infty})$ as $n \rightarrow \infty$

$$\left(\frac{1}{(2\sigma^2 nh)^{1/2}} \left[\sum_{i=\lfloor nt \rfloor + 1}^{\lfloor n(t+h) \rfloor} X_i - \sum_{i=\lfloor n(t-h) \rfloor + 1}^{\lfloor nt \rfloor} X_i \right] \right)_t \xrightarrow{d} (L_{t,h})_t,$$

where the constant μ vanishes. Now by replacing $2\sigma^2$ by $\hat{\sigma}_r^2 + \hat{\sigma}_\ell^2$ and using Lemma 3.1 and Slutsky's theorem weak convergence of $(D_{t,h}^{(n)})_{(t,h) \in \Delta_{\delta}}$ follows. \square

Proof of Lemma 4.2: Within A_u the slope of $(n^{-1/2} \cdot |d_{t,h}^{(n)}|)_t$ is positive left of c_u and negative right of it, see Lemma 3.3. Thus, $|t_s(k) - c_u| = |t_s - c_u| - (k+1) \Leftrightarrow |t_s - c_u| \geq k+1$ and (12) holds true. The path ends after $h_s - \delta$ steps, i.e., $t_e = c_u \Leftrightarrow |t_s - c_u| \leq h_s - \delta + 1 \Leftrightarrow (t_s, h_s) \in B_u$. Further, $(t_s, h_s) \in A_u$ implies $|t_s - c_u| \leq h_s$ (double window overlaps c_u), and thus $(t_s, h_s) \in A_u \setminus B_u$ implies $|t_s - c_u| \in \{h_s - \delta + 2, \dots, h_s\}$, hence $|t_e - c_u| = |t_s - c_u| - (h_s - \delta + 1) \in \{1, \dots, \delta\}$. \square

Proof of Proposition 4.3 From Corollary 3.2 we obtain a.s. as $n \rightarrow \infty$

$$\sup_{(t,h) \in \Delta_{\delta}} \left| |n^{-1/2} \cdot D_{t,h}^{(n)}| - |d_{t,h}^{(1)}| \right| \rightarrow 0. \quad (21)$$

On A_u (excluding $t = c_u$) a lower bound for the derivative of $(|d_{t,h}^{(1)}|)_t$ is given through $\kappa_a \delta^{1/2} > 0$, see Lemma 3.3. Thus, for any $\varepsilon > 0$ it is

$$|d_{t,h}^{(1)}| - |d_{t-\varepsilon,h}^{(1)}| \geq \kappa_a \delta^{1/2} \varepsilon, \quad \text{if } t \leq c_u, \quad \text{and} \quad |d_{t,h}^{(1)}| - |d_{t+\varepsilon,h}^{(1)}| \geq \kappa_a \delta^{1/2} \varepsilon, \quad \text{if } t > c_u, \quad (22)$$

provided that (t, h) , $(t - \varepsilon, h)$, $(t + \varepsilon, h)$ lie in A_u . Consider the initializing step of the path, $k = 0$. Both $\hat{t}_s^{(n)}(k)$ and $t_s(k)$ take a value in $\{t_s - 1, t_s, t_s + 1\} \cap \Delta_\delta$. As $\hat{t}_s^{(n)}(k)$ is a maximizer defined via $|D_{t,h}^{(n)}|$ we obtain $|n^{-1/2} \cdot D_{\hat{t}_s^{(n)}(k), h-k}^{(n)}| \geq |n^{-1/2} \cdot D_{t_s(k), h-k}^{(n)}| \rightarrow |d_{t_s(k), h-k}^{(1)}|$ a.s. as $n \rightarrow \infty$, where the convergence follows from (21), i.e.,

$$|n^{-1/2} \cdot D_{\hat{t}_s^{(n)}(k), h-k}^{(n)}| \geq |d_{t_s(k), h-k}^{(1)}| + o_{a.s.}(1). \quad (23)$$

From this we bound

$$\begin{aligned} |d_{t_s(k), h-k}^{(1)}| - |d_{\hat{t}_s^{(n)}(k), h-k}^{(1)}| + o_{a.s.}(1) & \\ & \leq |n^{-1/2} \cdot D_{\hat{t}_s^{(n)}(k), h-k}^{(n)}| - |d_{\hat{t}_s^{(n)}(k), h-k}^{(1)}| + o_{a.s.}(1) \\ & \leq \left| n^{-1/2} \cdot D_{\hat{t}_s^{(n)}(k), h-k}^{(n)} - d_{\hat{t}_s^{(n)}(k), h-k}^{(1)} \right| + o_{a.s.}(1) \\ & \leq \sup_{(t,h) \in \Delta_\delta} \left| n^{-1/2} \cdot D_{t,h}^{(n)} - d_{t,h}^{(1)} \right| + o_{a.s.}(1) \xrightarrow{a.s.} 0. \end{aligned} \quad (24)$$

In the first inequality we used (23), in the second the triangle inequality, and the convergence follows from (21). The estimator $\hat{t}_s^{(n)}(k)$ is now tied to the nonrandom function via $d_{\hat{t}_s^{(n)}(k), h-k}^{(1)}$, and (22) brings us from the function to the estimator. Let $\varepsilon > 0$. Then almost everywhere it holds that if $|t_s(k) - \hat{t}_s^{(n)}(k)| > \varepsilon$ i.o., thus $|d_{t_s(k), h-k}^{(1)}| - |d_{\hat{t}_s^{(n)}(k), h-k}^{(1)}| > \varepsilon \kappa_a \delta^{1/2}$ i.o. But as the latter only occurs finitely often it is $t_s(k) = \hat{t}_s^{(n)}(k)$ a.s. for n large. Iteratively, this extends for all $k = 1, 2, \dots, h - \delta$, i.e., eventually the paths w.r.t. $D_{t,h}^{(n)}$ and $d_{t,h}^{(n)}$ coincide a.s. \square

Proof of Lemma 4.4: From $\delta < \lfloor \delta_C / 2 \rfloor$ conclude that A_u contains a square \mathcal{S} with horizontal and vertical edges of length $\lfloor \delta_C / 2 \rfloor$: choose the center of \mathcal{S} as (c_u, δ_C) . In fact, the right corners of \mathcal{S} may only be adjacent to A_u . Nevertheless, $\mathcal{S} \cap S_{\lfloor \delta_C / 2 \rfloor} \neq \emptyset$, and thus $\mathcal{S} \cap S_g \neq \emptyset$ for $g \leq \lfloor \delta_C / 2 \rfloor$. \square

Proof of Theorem 4.6: For $(t_s, h_s) \in S$ set $\hat{t}_{e_s}^{(n)} := \hat{t}_e^{(n)}$, making the relation to $(t_s, h_s) \in S$ explicit. Let $C \neq \emptyset$. Then a.s. for n large enough it is

$$\max_{(t_s, h_s) \in S \setminus R} \left(\min\{|\hat{t}_{e_s}^{(n)} - c_u| : c_u \in C\} \right) \leq \delta - 1, \quad (25)$$

i.e., all potential paths that start in the 'upper part' $S \setminus R$ of Δ_δ end close to a $c_u \in C$. (25) holds true, as for any $(t_s, h_s) \in S \setminus R$ the path eventually enters an A_u and then Proposition 4.3 states a.s. $|\hat{t}_{e_s}^{(n)} - c_u| \leq \delta - 1$ for n large. The maximum follows from $|S|$ being finite. Further, a.s. for n large it is

$$\min_{(t_s, h_s) \in \bigcup_{u=1, \dots, |C|} A_u} [(nh)^{-1/2} \cdot |D_{t,h}^{(n)}|] > \max_{(t_s, h_s) \in R} [(nh)^{-1/2} \cdot |D_{t,h}^{(n)}|], \quad (26)$$

i.e., as long as the algorithm does not break, starting points are first chosen from $S \setminus R \supset \bigcup_u A_u$ up until all of them are cut out, and after that they are chosen from R . (26) follows from Corollary 3.2 and Lemma 3.3, noting that $d_{t,h}^{(1)} = 0$ if $(t, h) \in R$, and $|d_{t,h}^{(1)}| > 0$ if $(t, h) \in A_u$.

Combining (25) and (26), it follows that a.s. for n large at first all $c \in C$ are estimated

up to a distance $\delta - 1$ from starting values within $S \setminus R$, given the algorithm does not break. Possibly step 3a is applied in between. We need to show that the breaking criterion 3b applies appropriately: First, for $m \leq |C|$ we show that it does not apply. A path starting in $S \setminus R$ must pass an A_u such that a.s. for n large

$$\min_{(t_s, h_s) \in S \setminus R} \left[\max_{k=0, 1, \dots, h_s - \delta} |D_{\hat{t}_s^{(n)}(k), h_s - k}^{(n)}| \right] \geq \min_{(t, h) \in \bigcup A_u} |D_{t, h}^{(n)}| > n^\beta,$$

i.e., the maximum w.r.t. any path starting in $S \setminus R$ exceeds the minimum w.r.t. to all A_u , and the second inequality holds as $D_{t, h}^{(n)} = n^{1/2} d_{t, h}^{(1)} + o_{a.s.}(n^{1/2})$ uniformly on Δ_δ (Corollary 3.2) and $|d_{t, h}^{(1)}| > 0$ within all A_u (Lemma 3.3), noting that $\beta < 1/2$. Thus, a.s. for n large there is no break.

Second, for $m = |C| + 1$ the algorithm now breaks. All $c \in C$ are estimated. Thus, possibly after applying criterion 3a, all remaining starting points lie in R . This also covers $C = \emptyset$. Note that a path that starts in R remains in R . It holds a.s. for n large

$$\max_{(t_s, h_s) \in R} \left[\max_{k=0, 1, \dots, h_s - \delta} |D_{\hat{t}_s^{(n)}(k), h_s - k}^{(n)}| \right] \leq \max_{(t, h) \in R} |D_{t, h}^{(n)}| < n^{1/2-v},$$

i.e., the maximum w.r.t. all paths starting in R deceeds the maximum w.r.t the entire R . For the second inequality we note that within R it is $d_{t, h}^{(1)} = 0$ and thus $D_{t, h}^{(n)} = o_{a.s.}(n^{1/2-v})$ uniformly on R (Corollary 3.2). As $\beta \geq 1/2 - v$, a.s. for n large the algorithm breaks.

Finally note that 3c. is asymptotically redundant: a.s. for n large, for $m \leq |C|$ we stated correct estimation up to the error, so neighboring estimates will have at least distance $\delta_C - 2(\delta - 1)$, and for $m = |C| + 1$ the algorithm already broke in 3b. \square

References

- Antoch, J. and Hušková, M. (1999). Estimators of changes. In Asymptotics, nonparametrics, and time series, volume 158 of Statist. Textbooks Monogr., pages 533–577. Dekker, New York.
- Aston, J. A. D. and Kirch, C. (2012). Evaluating stationarity via change-point alternatives with applications to fmri data. Ann. Appl. Stat., 6(4):1906–1948.
- Aue, A. and Horváth, L. (2013). Structural breaks in time series. J. Time Ser. Anal., 34(1):1–16.
- Baranowski, R., Chen, Y., and Fryzlewicz, P. (2019a). Narrowest-over-threshold detection of multiple change-points and change-point-like features. J. R. Stat. Soc., B: Stat. Methodol., 81:649–672.
- Baranowski, R., Chen, Y., and Fryzlewicz, P. (2019b). not: Narrowest-Over-Threshold Change-Point Detection. R package version 1.2.
- Baranowski, R. and Fryzlewicz, P. (2019). wbs: Wild Binary Segmentation for Multiple Change-Point Detection. R package version 1.4.
- Berkes, I., Horváth, L., Kokoszka, P., and Shao, Q.-M. (2006). On discriminating between long-range dependence and changes in mean. Ann. Statist., 34(3):1140–1165.

- Brodsky, B. (2017). Change-point analysis in nonstationary stochastic models. CRC Press, Boca Raton, FL.
- Chen, J. and Gupta, A. K. (2000). Parametric statistical change point analysis. Birkhäuser Boston, Inc., Boston, MA.
- Cho, H. and Kirch, C. (2022). Two-stage data segmentation permitting multiscale change points, heavy tails and dependence. Ann Inst Stat Math, 74(4):653–684.
- Chu, C.-S. J., Hornik, K., and Kuan, C.-M. (1995). MOSUM tests for parameter constancy. Biometrika, 82(3):603–617.
- Csörgő, M. and Horváth, L. (1997). Limit theorems in change-point analysis. Wiley Series in Probability and Statistics. John Wiley & Sons, Ltd., Chichester. With a foreword by David Kendall.
- Dehling, H., Rooch, A., and Taqqu, M. S. (2017). Power of change-point tests for long-range dependent data. Electron. J. Stat., 11(1):2168–2198.
- Dette, H., Eckle, T., and Vetter, M. (2020). Multiscale change point detection for dependent data. Scand. J. Stat., 47(4):1243–1274.
- Döring, M. (2010). Multiple change-point estimation with U -statistics. J. Statist. Plann. Inference, 140(7):2003–2017.
- Eichinger, B. and Kirch, C. (2018). A mosum procedure for the estimation of multiple random change points. Bernoulli, 24(1):526–564.
- Fang, X., Li, J., and Siegmund, D. (2020). Segmentation and estimation of change-point models: false positive control and confidence regions. Ann. Statist., 48(3):1615–1647.
- Fryzlewicz, P. (2014). Wild binary segmentation for multiple change-point-detection. Ann. Statist., 42(6):2243–2281.
- Fryzlewicz, P. (2018a). Supplement to "tail-greedy bottom-up data decompositions and fast multiple change-point detection".
- Fryzlewicz, P. (2018b). Tail-greedy bottom-up data decompositions and fast multiple change-point detection. Ann. Statist., 46(6B):3390–3421.
- Gombay, E. and Horváth, L. (1994). An application of the maximum likelihood test to the change-point problem. Stochastic Process. Appl., 50(1):161–171.
- Gombay, E. and Horváth, L. (2002). Rates of convergence for U -statistic processes and their bootstrapped versions. volume 102, pages 247–272. Silver jubilee issue.
- Harchaoui, Z. and Lévy-Leduc, C. (2010). Multiple change-point estimation with a total variation penalty. J. Amer. Statist. Assoc., 105(492):1480–1493.
- Hinkley, D. V. (1971). Inference about the change-point from cumulative sum tests. Biometrika, 58(3):509–523.
- Holmes, M., Kojadinovic, I., and Quessy, J.-F. (2013). Nonparametric tests for change-point detection à la Gombay and Horváth. J. Multivar. Anal., 115:16–32.
- Horváth, L. and Hušková, M. (2005). Testing for changes using permutations of U -statistics. J. Statist. Plann. Inference, 128(2):351–371.

- Horváth, L. and Shao, Q.-M. (2007). Limit theorems for permutations of empirical processes with applications to change point analysis. *Stochastic Process. Appl.*, 117(12):1870–1888.
- Hušková, M. and Slabý, A. (2001). Permutation tests for multiple changes. *Kybernetika*, 37(5):605–622.
- Kass-Hout, T., Xu, Z., McMurray, P., Park, S., Buckeridge, D., Brownstein, J., Finelli, L., and Groseclose, S. (2012). Application of change point analysis to daily influenza-like illness emergency department visits. *JAMIA*, 19:1075–81.
- Killick, R., Eckley, I. A., Ewans, K., and Jonathan, P. (2010). Detection of changes in variance of oceanographic time-series using changepoint analysis. *Ocean Eng.*, 37(13):1120–1126.
- Killick, R., Haynes, K., and Eckley, I. A. (2016). *changepoint: An R package for changepoint analysis*. R package version 2.2.2.
- Lavielle, M. and Moulines, E. (2000). Least-squares estimation of an unknown number of shifts in a time series. *J. Time Ser. Anal.*, 21(1):33–59.
- Levajković, T. and Messer, M. (2021). *mscp: Multiscale Change Point Detection via Gradual Bandwidth Adjustment in Moving Sum Processes*. R package version 1.0.
- Li, H. and Sieling, H. (2017). *FDRSeg: FDR-Control in Multiscale Change-Point Segmentation*. R package version 1.0-3.
- Matteson, D. S. and James, N. A. (2014). A nonparametric approach for multiple change point analysis of multivariate data. *J. Am. Stat. Assoc.*, 109(505):334–345.
- Meier, A., Kirch, C., and Cho, H. (2021). *mosum: A package for moving sums in change-point analysis*. *J. Stat. Softw.*, 97(8):1–42.
- Messer, M. (2022). Bivariate change point detection: joint detection of changes in expectation and variance. *Scand. J. Stat.*, 49:886–916.
- Messer, M., Kirchner, M., Schiemann, J., Roeper, J., Neining, R., and Schneider, G. (2014). A multiple filter test for the detection of rate changes in renewal processes with varying variance. *Ann. Appl. Stat.*, 8(4):2027–2067.
- Muggeo, V. M. (2020). *cumSeg: Change Point Detection in Genomic Sequences*. R package version 1.3.
- Nurk, S., Koren, S., Rhie, A., Rautiainen, M., Bizkadze, A., Mikheenko, A., Vollger, M., Altemose, N., Uralsky, L., Gershman, A., Aganezov, S., Hoyt, S., Diekhans, M., Logsdon, G., Alonge, M., Antonarakis, S., Borchers, M., Bouffard, G., Brooks, S., Caldas, G., Chen, N., Cheng, H., Chin, C., Chow, W., de Lima, L., Dishuck, P., Durbin, R., Dvorkina, T., Fiddes, I., Formenti, G., Fulton, R., Functammasan, A., Garrison, E., Grady, P., Graves-Lindsay, T., Hall, I., N.F., H., Hartley, G., Haukness, M., Howe, K., Hunkapiller, M., Jain, C., Jain, M., Jarvis, E., Kerpedjiev, P., Kirsche, M., Kolmogorov, M., Korch, J., Kremitzki, M., Li, H., Maduro, V., Marschall, T., McCartney, A., McDaniel, J., Miller, D., Mullikin, J., Myers, E., Olson, N., Paten, B., Peluso, P., Pevzner, P., Porubsky, D., Potapova, T., Rogaev, E., Rosenfeld, J., Salzberg, S., Schneider, V., Sedlazeck, F., Shafin, K., Shew, C., Shumate, A., Sims, Y., Smit, A., Soto, D., Sović, I., Storer, J., Streets, A., Sullivan, B., Thibaud-Nissen, F., Turrance, J., Wagner, J., Walenz, B., Wenger, A., Wood, J., Xiao, C., Yan, S., Young, A., Zarate, S., Surti, U., McCoy, R., Dennis, M., Alexandrov, I., Gerton, J., O’Neill, R., Timp, W., Zook, J., Schatz, M., Eichler, E., Miga, K., and Phillippy, A. (2022). The complete sequence of a human genome. *Science*, 376:44–53.

- Page, E. S. (1954). Continuous inspection schemes. *Biometrika*, 41(1-2):100–115.
- Pein, F., Hotz, T., Sieling, H., and Aspelmeier, T. (2020). *stepR: Multiscale change-point inference*. R package version 2.1-1.
- Pein, F., Sieling, H., and Munk, A. (2017). Heterogeneous change point inference. *J. R. Stat. Soc. Ser. B Methodol.*, 79(4):1207–1227.
- Reeves, J., Chen, J., Wang, X. L., Lund, R., and Lu, Q. Q. (01 Jun. 2007). A review and comparison of changepoint detection techniques for climate data. *JAMC*, 46(6):900–915.
- Rybach, D., Gollan, C., Schluter, R., and Ney, H. (2009). Audio segmentation for speech recognition using segment features. In *2009 IEEE International Conference on Acoustics, Speech and Signal Processing*, pages 4197–4200.
- Spokoiny, V. (2009). Multiscale local change point detection with applications to value-at-risk. *Ann. Statist.*, 37(3):1405–1436.
- Steinebach, J. and Eastwood, V. R. (1995). On extreme value asymptotics for increments of renewal processes. volume 45, pages 301–312. *Extreme value theory and applications* (Villeneuve d’Ascq, 1992).

Contact information

Tijana Levajković

email.: tijana.levajkovic@tuwien.ac.at

Michael Messer

email.: michael.messer@tuwien.ac.at

Vienna University of Technology

Institute of Statistics and Mathematical Methods in Economics

Wiedner Hauptstraße 8-10/105

1040 Vienna, Austria